Utrecht University

Royal Netherlands Institute for Sea Research

CMIP6 model performance in the Subpolar North Atlantic in relation to the AMOC

MASTER THESIS

Erika Giorgi

Student Number: 7445822

Marine Sciences

Primary Supervisor: Dr. Femke de Jong (NIOZ)

Secondary Supervisor: Elodie Duyck (NIOZ)

Additional Supervisor: Dr. Peter Bijl (UU)

Date: February 10th, 2023

Abstract

In a warming climate, it is necessary to understand how the ocean, a crucial component of the climate system, will react. The Atlantic Meridional Overturning Circulation (AMOC) transports heat, nutrients, and carbon, but is often not well represented in climate models. Deep convection in the Subpolar North Atlantic (SPNA) influences the strength of this circulation and is an important feature to represent accurately in climate models for reliable future projections. This thesis explores how the representation of circulation and hydrography impacts stratification and regions of deep convection in the SPNA for a range of CMIP6 models in comparison to CMEMS reanalysis. All of the models show temperature and salinity biases throughout the Labrador, Irminger, and Nordic Seas, influencing the stratification and location or depths of deep convection. These biases can be caused by an overestimation of sea ice concentration, especially in the Labrador Sea, or too high temperatures in the North Atlantic Current with a stronger AMOC compared to observations. Increasing ocean resolution is not found to improve these biases, and results in an overestimation of the mixed layer depth in the Labrador Sea. If these processes are not well represented in comparison to observations or reanalysis products, it may influence their validity for future AMOC and climate projections.

Table of Contents

1. Introduction

Understanding the past evolution and dynamics of the climate system allows for better prediction of potential future events. The surface ocean is in direct contact with the atmosphere, and ocean circulation has implications for heat, nutrient, and carbon dioxide exchange and storage (Gruber et al., 2002; Lozier 2012). The North Atlantic Ocean is the largest carbon sink for the Northern Hemisphere, with carbon being stored at depth for several hundred to thousands of years (Sabine et al., 2004, Gruber et al., 2002 and references therein). A change in ocean circulation under global warming can therefore have severe impacts on the climate and ramifications for society. The need to better understand the ocean as part of the climate system has led to large observational and modelling efforts over the years. However, there are many uncertainties causing disagreement between various models and reduced confidence in their projections. This will be explored further in Section 1.5, but first, the components that make up the AMOC and why they can be so difficult for climate models to reproduce will be discussed.

1.1 Atlantic Meridional Overturning Circulation

The Atlantic Meridional Overturning Circulation (AMOC) transports warm, salty waters poleward on the surface and cold, dense waters equatorward at depth. The overturning circulation is forced by density differences from temperature and salinity causing deep vertical mixing and sinking in the high latitudes, as well as by surface winds inducing upwelling (Killworth, 1983, Kuhlbrodt et al., 2007 and references therein). The 'upper cell' in the North Atlantic is responsible for the ventilation of the upper ~ 2000 m of the ocean, with the formation of the North Atlantic Deep Water (NADW) transporting and storing carbon-rich waters. The 'lower cell' emanates from Antarctica, flowing deep into the abyssal ocean forming the Antarctic Bottom Water (AABW; Buckley & Marshall, 2016 and references therein).

The AMOC influences many parts of the climate system. The warm ocean surface circulation supplies heat to the northern hemisphere, and westerly winds transport this heat toward the UK and Europe, allowing for milder temperatures compared to similar latitudes in North America (Trenberth & Caron, 2001, Levermann et al., 2012). With a warming climate, there is an increased risk of more meltwater from the Greenland ice sheet (GrIS) and Arctic sea ice, which would result in a freshening of the North Atlantic. Additionally, warmer atmospheric temperatures allow for less heat loss from the ocean surface. Warmer or fresher waters result

in an increased water column stratification, decreasing the potential for deep convection and can reduce the strength of the overturning circulation (e.g., Thorpe et al., 2001). Such an AMOC decline could impact global and regional climates by affecting temperatures, precipitation, sea level, and Arctic sea ice extent, just to name a few (e.g., Jackson et al., 2015, Kuhlbrodt et al., 2007 and references therein, Buckley & Marshall, 2016 and references therein, McCarthy et al., 2017).

The latest IPCC AR6 report states that "the AMOC will decline over the 21st century (high confidence, but low confidence for quantitative projections)" but with "low confidence in reconstructed and modelled AMOC changes for the 20th century" (IPCC, 2022). Some observational studies and model simulations indicate this slowdown may already be in effect, although more data is required over a longer period to assess the variability (e.g., Frajka-Williams 2015). Models used to make these predictions suffer from several uncertainties, such as how much the Greenland ice sheet will decrease in a warming climate, and how this freshwater will potentially impact deep convection in the North Atlantic and contribute to AMOC slowdown. If interactions between the ice, ocean, and atmosphere are not fully considered in a climate model, or the pathways of cold and fresh or warm and saline water are incorrectly represented, this can create further uncertainty in the projections. The focus of this thesis is in the Subpolar North Atlantic because of the variability associated with the AMOC and uncertainties in freshwater input or heat transport to the region, described further in the next section.

1.2 Subpolar North Atlantic

The Subpolar North Atlantic (SPNA) is an important region for deep convection and overturning circulation. The region spans various basins, shown in Figure 1, with the Labrador Sea between Canada and west Greenland, the Irminger Sea between east Greenland and the Reykjanes Ridge (RR), and the Iceland Basin on the eastward side of the RR. Further north of Iceland are the Nordic Seas (or Greenland-Iceland-Norway, GIN Seas not shown here). The subpolar gyre spans the Irminger and Labrador Seas, with a cyclonic circulation preconditioning the water column for deep convection.

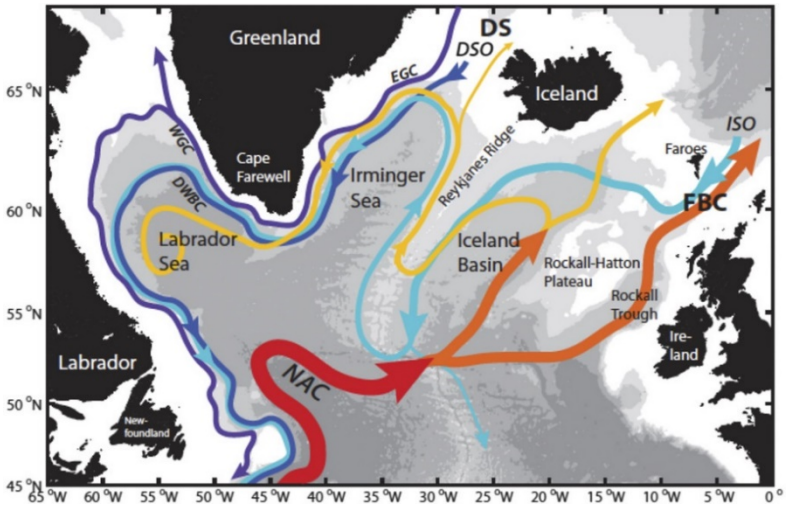

Figure 1: Representation of the large-scale currents in the Subpolar North Atlantic. Colors indicate relative water temperature (from the warm North Atlantic Current (NAC) in red branching into orange and yellow currents, with the coldest currents in light blue and purple such as Denmark Strait Overflow Water (DSOW) at depth and East Greenland Current (EGC) on the shallow Greenland shelf. Credit: H. Furey, Woods Hole Oceanographic Institution. Adapted from Lozier et al. (2017).

The warm and saline North Atlantic Current (NAC; Fig.1 red arrow) connects the subtropic and subpolar gyres, flowing northwards from the pathway of the Gulf Stream and splitting up into multiple trajectories further north. Some of this water enters the eastern Irminger Sea as the Irminger Current (yellow arrow in the Iceland and Irminger Basins, Fig. 1), steered northwards by the Reykjanes Ridge (RR) and flows along the east Greenland shelf into the Labrador Sea, transporting relatively warm and saline waters into this region (Våge et al., 2011). Cooler and denser waters are represented by blue and purple arrows in Figure 1, such as the Denmark Strait Overflow Water (DSOW) originating in the Nordic Seas, the Deep Western Boundary Current (DWBC), and the West Greenland Current (WGC) into the Labrador Sea. Cold and fresh meltwater from the Arctic enters the SPNA through the Denmark Strait (DS) and flows along the shallow (~ 500 m) east Greenland shelf as the East Greenland

Current (EGC) and East Greenland Coast Current (EGCC), first described by Bacon et al. (2002).

The EGC is a narrow (~ 50 km), cold (~ 0 °C) current with varying salinities (practical salinity between 30 and 35) connecting the Arctic and North Atlantic oceans (Aagaard & Coachman, 1968a, 1968b, Sutherland & Pickart, 2008). This current is at the front between the cool Arctic waters flowing from Fram Strait in the north and warmer saline waters flowing in from the NAC. Closer to the Greenland coast, the EGCC is an even narrower (~ 20 km) freshwater (practical salinity between 28 and 34) current containing both Arctic waters and runoff from Greenland (Bacon et al., 2002). These small-scale currents can be difficult to resolve in climate models but are important for the transport of fresh and cold waters which can be exported into the North Atlantic. With cold water temperatures, density is controlled significantly more by salinity, and changes in this impact the water column stratification. This makes it important to study in relation to deep convection and consequently the overturning strength in a changing climate.

1.3 Deep Convection

The ocean is generally stably stratified, with lighter surface waters and increasing density with depth. Winds and waves cause turbulence, creating a shallow mixed layer down to 50 – 100 m with homogeneous properties such as temperature and salinity (Lazier et al., 2001). If the surface waters become denser than the underlying waters, then mixing and sinking can occur. This can happen when the surface waters lose or exchange heat with the atmosphere or by an increase in salinity through evaporation or formation of sea ice and brine rejection, ultimately resulting in surface buoyancy loss (Lozier, 2012). The formation of a mixed layer deeper than ~ 1000 m is referred to as "deep" convection (Talley, 2011).

Marshall and Schott (1999) provide one of the first representations of deep convection and stages of mixing in the ocean. The process is described in three phases, shown in Figure 2 as (a) preconditioning, (b) onset of deep convection, and (c) lateral exchange and eventually restratification with export of the convective water mass downwards.

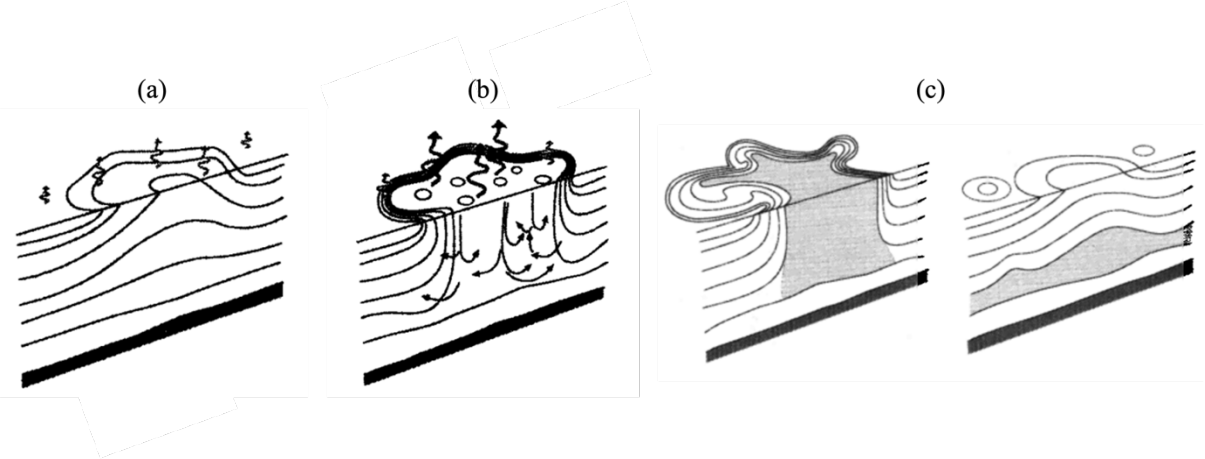

Figure 2: Schematic diagram of the three phases of open-ocean deep convection: (a) preconditioning, (b) deep convection, and (c) lateral exchange and spreading. Buoyancy flux through the sea surface is represented by curly arrows, and the underlying stratification/outcrops is shown by continuous layers. The volume of fluid mixed by convection is shaded. Adapted from Marshall & Schott (1999).

During the first phase of preconditioning (a), the upper water column stratification begins to be disrupted by a loss of surface buoyancy. The cyclonic circulation of the subpolar gyre creates a 'doming' of the isopycnals, bringing less stratified deeper waters towards the surface (Marshall & Schott, 1999; Lazier et al., 2001; Sgubin et al., 2017). The horizontal scale of this process can be from tens to hundreds of kilometres and occurs over various timescales between weeks to even years (Vreugdenhil & Gayen, 2021). For deep convection to occur, there must be a weak initial density stratification alongside a strong surface buoyancy forcing such as by intense wind events (de Jong, et al., 2018). During deep convection (b), convective plumes start

to form vertically in the water column as dense waters sink through layers of lighter water. The final stage, lateral exchange and spreading (c), is caused by a lateral mixing of dense waters and eventually restratification in the summer. The darker shading in Figure 2c shows the "volume of fluid mixed by convection" and depicts the sinking of dense waters to depth (Marshall & Schott, 1999).

Deep convection regions in the Labrador and Irminger Seas are located near land, with cold and intense winds increasing the heat loss to the atmosphere from the surface ocean (Lazier et al., 2001). This cooling effect must be stronger than the freshening (decrease in salinity) of the waters, which reduces the density, otherwise mixing cannot occur due to the stable high stratification. The depth of this mixed layer varies between years, extending down to several hundreds of meters, or more than 1 km depth with strong forcing conditions (e.g., Våge et al., 2008; de Jong & de Steur, 2016; de Jong et al., 2012, 2018).

While global climate models can represent ocean processes relatively well, low spatial resolution is a limiting factor for smaller-scale physical processes. Parameterizations are often used, for example for eddies and overflow waters, but do not always accurately represent mixing processes. This can potentially impact the reliability of models and their projections for deep convection and consequently the AMOC. For example, in recent CMIP6 climate models (mostly with 100 km ocean horizontal resolution) used in IPCC reports, the depth of the mixed layer indicating the region of deep convection is largely over-estimated to unrealistic depths even down to the bottom of the seafloor (Heuzé, 2021).

1.4 Irminger Sea and Freshwater Fluxes

Most previous studies on AMOC variability and deep convection have been focused on the Labrador Sea (e.g., Gelderloos et al., 2012, Yang et al., 2016). Even though some studies (e.g., Pickart et al., 2003a, 2003b) have measured deep convection in the Irminger Sea, its importance to the AMOC was only determined more recently with additional observational studies (e.g., OSNAP; Lozier et al., 2019 and RAPID/MOCHA; Smeed et al., 2019). These studies have shown that the Irminger Sea contributes more to the total overturning strength than the Labrador Sea (Petit et al., 2020). The region of dense water formation in the Irminger Sea is significant for the variability in overturning circulation and has been studied more extensively in the last years (e.g., de Jong et al. 2018, de Jong & de Steur, 2016, Våge et al., 2011). In the interior Irminger Sea, the site of deep convection generally occurs just east of Cape Farewell, shown in Figure 3, depending on the stratification condition from the previous year (e.g., Pickart et al., 2003a, de Jong et al., 2012, Våge et al., 2008, 2011).

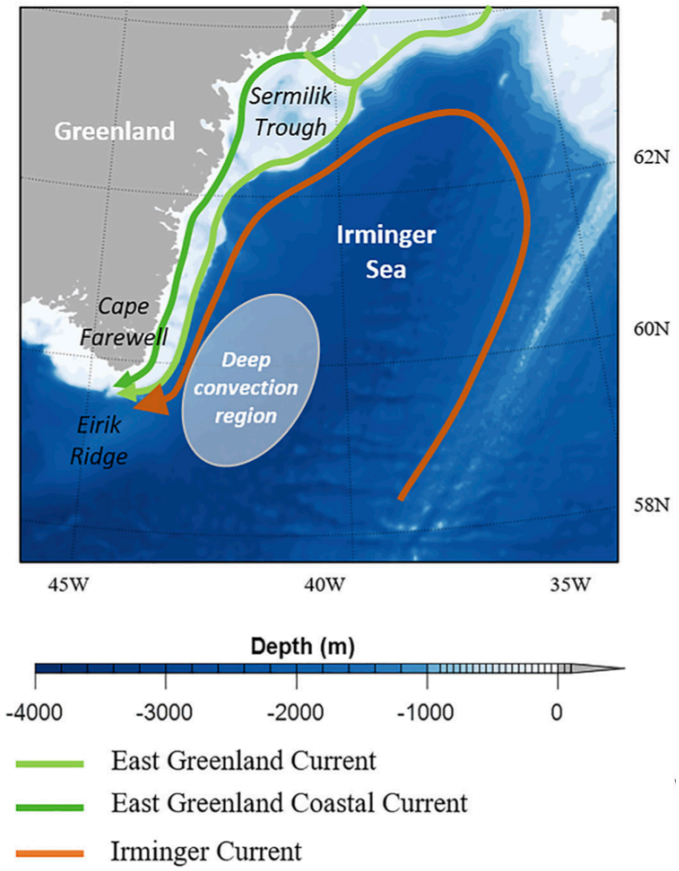

Figure 3: Site of deep convection in the Irminger Sea, south of Cape Farewell. Currents are indicated by the coloured lines. Adapted from Duyck, Gelderloos, and Jong (2022).

Significant to deep convection in this region are the Greenland tip jets (Moore, 2003). These are characterised by extremely strong north-westerly winds caused by the steep topography of Greenland and influenced by the North Atlantic Oscillation (NAO) low-pressure system (Pickart et al., 2003b, Moore, 2003, Moore & Renfrew, 2005). These events can drive heat exchanges between the surface ocean and atmosphere, contributing to buoyancy loss and deep convection (Pickart et al., 2003a 2003b; Våge et al., 2008). However, it is still relatively unknown how these tip jet events impact the stratification and deep convection in this region. These localized phenomena and surface forcings between the sea and atmosphere can further influence the strength of the overturning circulation and have important consequences for the climate but are not always well-represented in climate models.

Observations in the North Atlantic, especially during winter, are notoriously difficult due to the harsh climate. Therefore, there is a large reliance on climate models for a complete understanding of the evolution of ocean processes. Coupled climate models have the advantage of being able to reproduce various aspects of the global climate system as a whole, however, this also increases the potential for errors and uncertainties. Additionally, the sensitivity of the AMOC to an increase in freshwater inputs is still a large source of debate (Bakker, 2022). For low-resolution climate models, the heat and freshwater fluxes may not be accurately represented, thus impacting the accuracy and stability of the AMOC. These uncertainties and differences between models result in a range of projections of how the AMOC will respond to climate change (explored in the next section). Often, the multi-model mean projection is chosen to represent our best estimate of how the AMOC will evolve. However, if the model mean includes simulations that are unable to properly represent the properties and dynamics of the Subpolar North Atlantic, it should be considered whether to include them. Therefore, we want to evaluate the skill of several climate models in simulating the conditions and circulation in this region.

1.5 Previous CMIP6 Studies on AMOC strength and variability

Several studies have been performed with coupled climate models such as CMIP6, looking at the North Atlantic Deep Water formation (Heuzé, 2021) and how ocean resolution impacts the AMOC mean state (Jackson et al., 2020). Weijer et al. (2020) describe the AMOC as being a fundamental indicator for the performance of a climate model and is necessary for the reliability of its future projections. In their work, Weijer et al. (2020) study 27 CMIP6 models, for both historical and future scenarios. Figure 4 shows the strength of the AMOC at 26 °N in the models compared to the mean RAPID observational array between 2005 – 2014. Transport is given in Sverdrups (Sv), where 1 Sv = 10^6 m^3 s^{-1}.

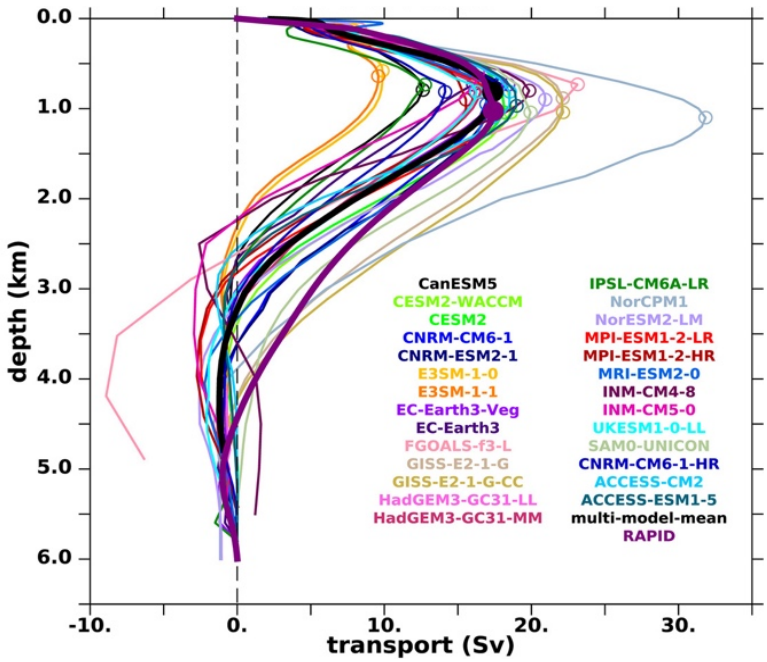

Figure 4: Mean overturning stream function at 26°N (averaged over 2005 - 2014). The ensemble mean is represented by the thick black line, the RAPID array is shown as a thick purple line. Adapted from Weijer et al., 2020.

While the multi-model-mean (thick black line in Figure 4) lies close to the RAPID mean for the peak transport at 1 km depth, the individual models show a range of strengths. Most notable from this figure is the NorCPM1 model with a peak transport above 30 Sv, more than double the RAPID transport mean (~ 17 Sv). The models with the lowest transports are E3SM-1-0 and E3SM-1-1 with a peak below 10 Sv. Some of the models closest to the RAPID peak are CESM2 and ACCESS-CM2, which will be studied in this work along with NorCPM1, CanESM5, and HadGEM3-GC31-LL (described further in Section 2.1).

For these models in Figure 4, the projected AMOC decline in the 21st century also varies significantly. Most of the models project a 34 – 45 % decline in the AMOC corresponding to

a decrease of 6 – 8 Sv, but a smaller selection of models only projects a weakening of up to 30 % (Weijer et al., 2020). This highlights the importance of studying various models and AMOC-related processes to achieve the most accurate projections. However, even though a model may perform well in comparison to observations, it is not an indicator of how well it will behave in the future but can be used to calibrate the models for the best estimate in their projections (Weijer et al., 2020).

If we want to know more about AMOC-related processes in these CMIP6 models, we can focus on particular regions, such as the Nordic, Irminger, and Labrador Seas, where deep convection occurs. For this, we consider the work by Heuzé (2021), analysing the representation of NADW formation, another important feature in climate models that is often difficult to represent. Heuzé (2021) determine where the models convect, and to what depths, using the mixed layer depth (MLD) when provided or calculating it themselves (see Heuzé 2021 and references therein). It was found that of all the 35 CMIP6 models studied, none were able to accurately represent the locations and depths of deep convection. The models are forming bottom waters "*too deeply, too often and/or over too large an area"* (Heuzé 2021). Various models convect in different regions, such as the Labrador Sea and Irminger Seas (separately or as one subpolar gyre) and the Nordic Seas. The maximum MLDs are mostly deeper than 1000 m, with some models even convecting to the sea floor. Dense bottom waters are formed also in the Nordic Seas and overflow over the Denmark Strait in the real ocean. These waters are incredibly dense, and only form a shallow bottom layer that is difficult to represent in coarser models, especially as the vertical resolution generally decreases with depth.

Comparing the capabilities of higher resolution models to lower resolution can be an indicator of the importance of small-scale processes, and to determine if they are better represented with ocean physics rather than parametrizations. This was explored in work by Jackson & Petit (2022). In their work, they compare low (100 km) and medium (25 km) ocean resolution for HadGEM3-GC31-LL and -MM, respectively. One notable difference between the models is the strength of the overturning, shown in Figure 5.

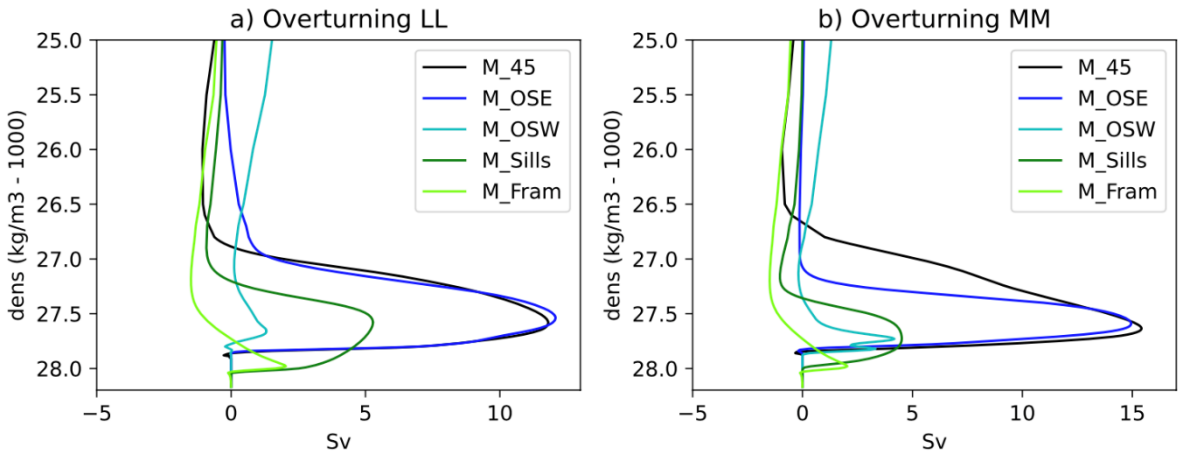

Figure 5: Overturning across sections (M_45: across the Atlantic at 45 °N, M_OSE: OSNAP east, M_OSW: OSNAP west, M_Sills: Greenland to Scotland sills, M_Fram: Fram strait) in density space. (a) Had-GEM3-GC31-LL (low-resolution model) and (b) Had-GEM3-GC31-MM (medium-resolution model). Adapted from Jackson and Petit (2022).

From Figure 5, both models have a strong overturning maximum at OSNAP east of ~ 12 Sv (LL) and 15 Sv (MM). For the OSNAP west section, the overturning is similar between both models (~ 5 Sv) with significantly reduced overturning compared to OSNAP east. The resolution of an ocean model can thus limit the representation of the AMOC due to the smaller-scale processes (such as, for example, overflow waters, eddy mixing or boundary currents) not being incorporated accurately (Jackson & Petit, 2020). Other processes which may be represented differently in models of various resolutions are interactions between model components such as the atmosphere, sea ice, and the ocean. Heat exchange between the ocean surface waters and the atmosphere can be hampered by the presence of sea ice, as well as through freshwater fluxes (e.g., runoff from Greenland and the Arctic or precipitation), affecting the stratification (Jackson & Petit, 2022 and references therein). These effects can lead to model biases at different resolutions and will be explored in the second part of this thesis.

1.6 Research Questions

This thesis aims to determine how winter conditions and processes in the Subpolar North Atlantic are represented in a range of CMIP6 models, and how this impacts deep convection. The results are compared to the CMEMS reanalysis product to test their validity.

To guide this research, we pose the following research question:

How does the representation of circulation and hydrography influence deep convection in a range of CMIP6 models?

To help answer this, we will answer the following sub-questions:

1. *How are winter sea surface temperature and salinity represented?*
2. *How do buoyancy differences from summer to winter influence mixed layer depths?*
3. *How does resolution impact the model performance in relation to deep convection?*

This thesis is structured as follows. Section 2 describes the selection of CMIP6 models (Section 2.1), CMEMS reanalysis (Section 2.2) and methods (Section 2.3). Section 3 presents the results, first for the low-resolution models with SPNA field maps of surface variables, stratification, and mixed layer depth (Section 3.1), then for hydrographic sections (Section 3.2). Section 3.3 compares low (LL) and medium (MM) resolution for the HadGEM3-GC31 model for SPNA field maps and hydrographic sections in Section 3.4. Section 4 is the summary and discussion, considering previous work on AMOC projections in CMIP6 models. The conclusions are presented in Section 5.

2. Models, Data, and Methods

2.1 Selection of CMIP6 Models

The Coupled Model Intercomparison Project Phase 6 (CMIP6) is the latest generation of global climate models, a combined international effort on behalf of climate modelers (Eyring et al., 2016). A selection of five models with different characteristics is made, considering work of Heuzé (2021) for deep convection locations and Weijer et al. (2020) for AMOC strengths. For one model, both low and medium resolutions for the ocean are considered to investigate the impact of increasing resolution. Model outputs are compared to the CMEMS reanalysis product, described in Section 2.2.

All models have variant-id r1i1f1p1, where r: realization (ensemble member), i: initialization, f: forcing, p: physics index, with the number indicating the configuration, except for the HadGEM3 models, for which this ensemble was not available and so the r1i1f1p3 is selected. This is to minimize the bias in the selection of models, as well as allowing for a more direct comparison with results by Heuzé (2021). Each CMIP6 model has the same historical forcings based (where possible) on observations from the period 1850 – 2014 (Eyring et al., 2016).

More model features and components are outlined in Table 1, showing the model name and data reference, atmospheric model component and resolution, ocean model component and resolution, number of ocean levels and vertical resolution, and the sea ice component.

Table 1: Selection of CMIP6 Model with model name (source id) and reference, atmospheric component, atmospheric resolution, ocean component, ocean resolution, ocean levels (and vertical resolution), and sea ice component. Adapted from https://wcrp cmip.github.io/CMIP6_CVs/docs/CMIP6_source_id.html.

Source id	Atmos	Res Atmos (km)	Ocean	Res Ocean (km)	Ocean Levels (vertical res)	Sea Ice
ACCESS-CM2 (Dix et al., 2019)	MetUM	250	MOM5.1	100	50 (10–333 m)	CICE5.1.2
CanESM5 (Swart et al., 2019b)	CanAM5	500	NEMO3.4.1	100	50 (6-250 m)	LIM2
CESM2 (Danabasoglu et al., 2019)	CAM6	100	POP2	100	60 (10–250 m)	CICE5.1
NorCPM1 (Bethke et al., 2019)	CAM-OSLO4.1	250	MICOM 1.1	100	51	CICE4
HadGEM3-GC31-LL (Ridley et al., 2019a)	MetUM-HadGEM3-GA7.1	250	NEMO-HadGEM3-GO6.0 (N96ORCA1)	100	75 (1-200 m)	CICE-HadGEM3-GSI8
HadGEM3-GC31-MM (Ridley et al., 2019b)	MetUM HadGEM3-GA7.1	100	NEMO-HadGEM3-GO6.0 (eORCA025)	25	75 (1-200 m)	CICE-HadGEM3-GSI8

More detailed information about each model and its components is summarised below:

- **ACCESS-CM2:** Convects both in the Labrador and Irminger seas separately, down to 2500 m (Heuzé, 2021). The maximum MLD (mean over a 30-year period) in the SPG is 2550 and 3623 m in the GIN Seas (Heuzé, 2021). The grid is orthogonal curvilinear, with a tripolar grid used above 65 °N. More information can be found at Bi et al. (2020) and references therein**.**
- **CanESM5**: Convects only in the Irminger Sea for a depth just beyond 1000 m (Heuzé, 2021). The depth of the maximum MLD in the SPG is 1269 m and 3216 m in the GIN seas (Heuzé, 2021 Appendix C). More information can be found at Swart et al. (2019a) and references therein.
- **CESM2:** Convects in both the Labrador and Irminger Seas as part of one subpolar gyre, however, the convection is too deep (beyond 2500 m) to be considered realistic (Heuzé, 2021). The depth of the maximum MLD in the SPG is 2280 m and 2017 m in the GIN seas (Heuzé, 2021 Appendix C). Contains an overflow parametrization for Denmark Strait Overflow Waters (DSOW). More information can be found at Danabasoglu et al. (2020) and references therein.
- **NorCPM1:** Deep convection only in the Labrador Sea, with a realistic depth of up to 1000 m (Heuzé, 2021). The maximum MLD depth in the SPG is 1005 m (Heuzé, 2021 Appendix C). More information can be found in Bethke et al. (2021) and references therein.
- **HadGEM3-GC31-LL:** Deep convection occurs both in the Labrador and Irminger Seas (separate regions) (Heuzé, 2021). The depth of convection is far too deep, reaching almost down to the bottom in both regions (Heuzé, 2021). More information can be found in Kuhlbrodt et al. (2018) and references therein.
- **HadGEM3-GC31-MM**: Eddy-resolving. Stronger overturning across OSNAP East than LL (Jackson & Petit, 2022). More information can be found in Williams et al. (2018) and references therein.

Model Variables and Definitions

The model variables used in this study are ‘thetao’ (potential temperature in °C), ‘so’ (practical salinity), ‘mlotst’ (mixed layer thickness in metres), ‘siconc’ (sea ice concentration, or the percentage of area covered by sea ice), ‘vo’ (the meridional ocean velocity). The MLD is

defined (for CMIP6 convections) as the depth where the monthly-mean potential density exceeds that at the surface by more than 0.125 kg m^{-3}. The model bathymetry is shown with 'deptho'. Conservative temperature and absolute salinity as calculated using TEOS-10, and these components are used to calculate the potential density (McDougall & Barker, 2011).

2.2 Reanalysis Data

Reanalysis is one of the best tools to obtain a complete view of the climate for historical data. Data assimilation techniques incorporate models and observations and can be compared with the performance of a coupled climate model to test their validity. We use the CMEMS GLORYS12V1 reanalysis (more information at: https://doi.org/10.48670/moi-00021) to compare to the CMIP6 models. The data assimilation used in CMEMS is altimeter data for sea level, satellite sea surface temperature and sea ice concentration, and in-situ TS profiles. The product is an eddy-resolving (1/12° horizontal resolution with 50 vertical levels) combination of models and observations. The ocean model is NEMO, which is of the same family as the CanESM5 CMIP6 model (NEMO3.4.1). Atmospheric forcing is provided by ERA5 reanalysis for recent years. We use monthly-mean data from January 1993 to March 2014. In the Irminger Sea, the CMEMS has been validated with two years of mooring data (de Jong et al., 2020). From this dataset, the monthly mean potential temperature, practical salinity, meridional ocean velocity, mixed layer thickness (with a density threshold of 0.03 instead of 0.125 kg m^{-3} as used in CMIP6), and sea ice concentration are downloaded for either surface layer throughout the SPNA or OSNAP East hydrographic section and analysed in Python.

2.3 Methods

The model data for each variable was downloaded using Pangeo from the online database ESGF (https://esgf-data.dkrz.de/projects/cmip6-dkrz/). Data between 1993 – 2014 is selected to best correspond to CMEMS and available observational data sets. The variables are sliced to the relevant region of the SPNA, the winter months of January, February, and March (JFM) or for the summer, July, August, and September (JAS) are selected, and the seasonal mean is taken for the entire dataset. For the field maps of temperature and salinity throughout the SPNA, the surface layer is selected, which is not at the same vertical depth level for the models.

The hydrographic section is taken approximately across the OSNAP East array, with initial position [60 °N, 47 °W] and ending at [57 °N, 14 °W], see Figure 10 for a visualization of the

line. To extract vertical sections at the same location for all the models, they each had to be re-gridded onto a 1 x 1 regular grid (0.25 x 0.25 for HadGEM3-GC31-MM). This is done with the xESMf Regridder. MetPy cross-section is then used to obtain the cross-sections.

To quantify the stratification to identify where deep convection can occur during the winter months, the buoyancy content of the upper 500 m of the water column is calculated. The water column buoyancy content *B* is calculated as follows (Equation 1, Biló et al., 2022):

$$B = \frac{g}{\rho_0} \int_0^z \left(\sigma_{0_z} - \sigma_0\right) dz, \tag{1}$$

where z is the vertical coordinate pointing toward the ocean bottom, $g = 9.8\, m\, s^{-2}$ the acceleration due to gravity, $\rho_0 = 1{,}027\ kg\ m^{-3}$ a reference density, σ_0 the potential density at the surface and σ_{0_z} the potential density at depth = z (Biló et al., 2022).

3. Results

In order to study the processes related to deep convection in the Subpolar North Atlantic, we first show the surface mean field for temperature and salinity. These variables determine the density stratification of the water, important for the location and intensity of deep convection. As deep convection occurs in the winter, the mean of the winter months is shown, unless stated otherwise. The summer variables for the surface mean fields are shown in Appendix 1.2.

3.1 Surface Mean Fields of the SPNA

Surface temperature and salinity indicate important processes such as locations of warm or cold currents and fronts. We compare the five CMIP6 surface mean fields to each other and to the CMEMS reanalysis for winter (JFM) 1993 - 2014. First, the three-month mean of sea surface temperature (SST) is shown in Figure 6. For the same time period and JFM mean, the sea ice concentrations are shown as contour lines, with values of 5, 50 and 90 % for the percentage of the grid cell covered by sea ice. The black box highlights the CMEMS output.

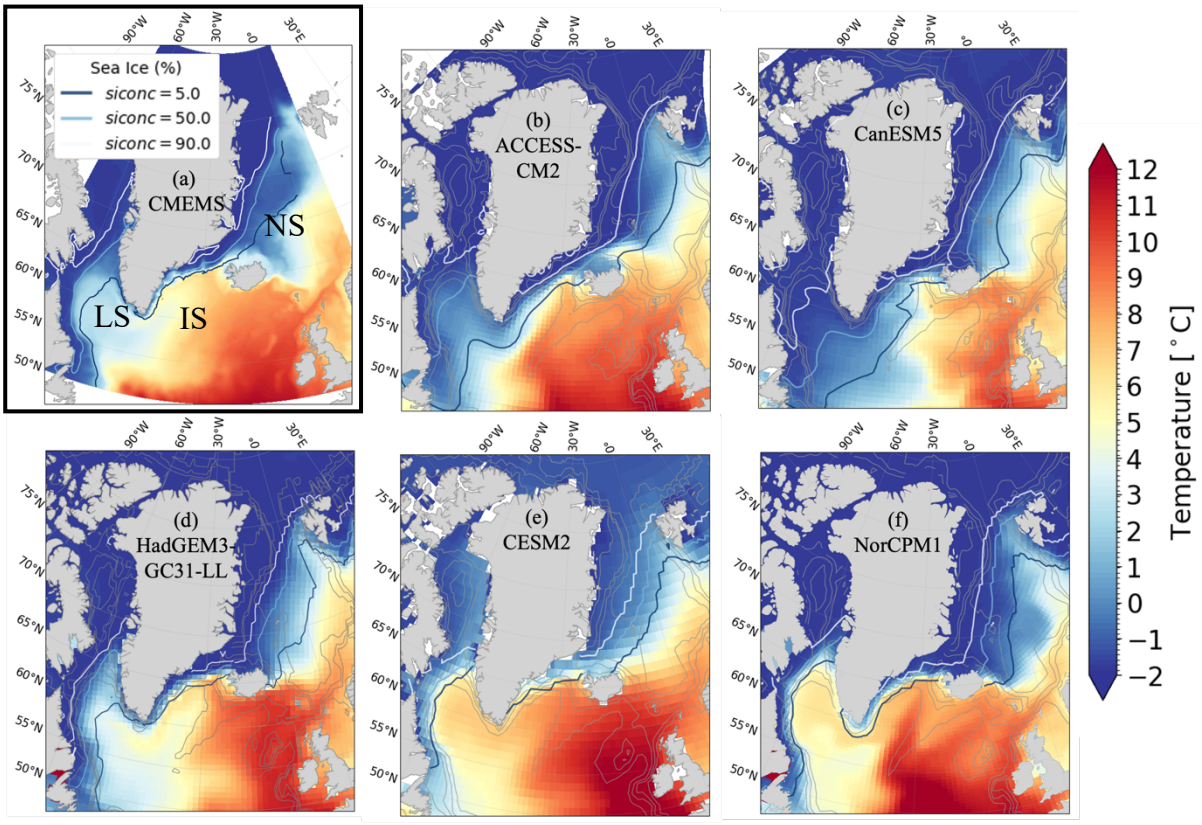

Figure 6: (a) Mean winter (JFM) CMEMS SST (°C) from 1993 to 2014 with labelled LS: Labrador Sea, IS: Irminger Sea, NS: Nordic Seas, (b-f) Model mean winter (JFM) 1993 - 2014 SST (°C). Temperatures are between -2 and 12 °C. Sea ice concentration (siconc) is shown as contour lines for 5, 50 and 90 %, indicating the percentage of the grid cell covered by ice. Isobaths in grey at 200, 500, 1000, 2000, 5000 m.

As discussed in the introduction, warm saline surface waters enter the SPNA through the North Atlantic Current (NAC). This is contrasted by fresh and cold waters from the Arctic. These currents can determine the density of the water by various temperature and salinity fluxes and should thus be well-represented in climate models for an accurate representation of deep convection. The mean sea surface temperature (SST) for the models (Fig. 6b-f) and reanalysis (Fig. 6a) shows a warm (up to 12 °C) region in the lower east SPNA characteristic of the NAC. This warm current extends northwards past Iceland on the eastward side and extends into the Nordic Seas, bringing warm surface waters to the high latitudes. In all cases, temperatures are lowest in the Arctic Sea, down to -2 °C with high concentrations of sea ice (> 90 %). This cold water enters the North Atlantic through Fram Strait (between Greenland and Svalbard), as well as through the Canadian Archipelago, following the coast of Greenland towards the south.

The models show a range of SSTs across the SPNA, with the most notable differences in the warm water entering from the NAC into the lower SPNA. Of all the models here, the highest temperatures throughout the lower east SPNA are in CESM2 (Fig. 6e) and NorCPM1 (Fig. 6f). These two models have a stronger AMOC at 26 °N than the RAPID mean (see Figure 4), much stronger in the case of NorCPM1 (Weijer et al., 2020). A stronger AMOC supplies more heat to high latitudes compared to a weaker AMOC, as shown in these two models. This warm water extends westward into the Labrador Sea with slightly reduced temperatures and shows a warm bias in this region compared to the other models and reanalysis. CESM2 and NorCPM1 also have the lowest sea ice concentration in the Labrador Sea compared to the other models and reanalysis. CanESM5 (Fig. 6c) has the lowest SST throughout the lower SPNA, with relatively lower NAC temperatures and much cooler Labrador Sea water. These cool Labrador Sea waters are also seen in ACCESS-CM2 (Fig. 6b), but the lower SPNA has higher temperatures compared to CanESM5. Both of these models (CanESM5 and ACCESS-CM2) have a cold bias in the Labrador Sea, with high concentrations of sea ice and a cold bias extending into the North Atlantic. CanESM5 has the lowest AMOC strength out of the models studied here, but ACCESS-CM2 has a similar or even higher peak transport than the RAPID mean, indicating more of a bias in the sea ice rather than AMOC strength (Weijer et al., 2020).

Most models show colder waters extending from the Arctic following the coast of Greenland by the pathway of the East Greenland Current (EGC). Only for CESM2 (Fig. 6e) this is not the case, with warm waters throughout the Irminger and Labrador Seas. This model has a similar AMOC strength to the RAPID mean (Weijer et al., 2020), indicating an underestimation of sea

ice in the Labrador Sea leading to warmer temperatures. Two models, ACCESS-CM2 (Fig. 6b) and CanESM5 (Fig. 6c) show extensive cold water eastward into the SPNA, while for HadGEM3-GC31-LL (Fig. 6d) and NorCPM1 (Fig. 6f), the cold water is contained on the shelf more closely resembling the EGC as seen also in CMEMS (Fig. 6a). Overall, HadGEM3-GC31-LL appears to most closely represent the CMEMS reanalysis product, with the exception of the North Atlantic Corner (warmer waters near Canada) which is notoriously difficult to resolve in lower resolution climate models.

Warm water currents entering the SPNA are associated with the NAC, which is also saline. Meanwhile, cold water currents are associated with fresh Arctic water. Therefore, similar patterns in the salinity as in the temperature may be observed in these two surface variables. The sea surface practical salinity (SSS) is shown in Figure 7.

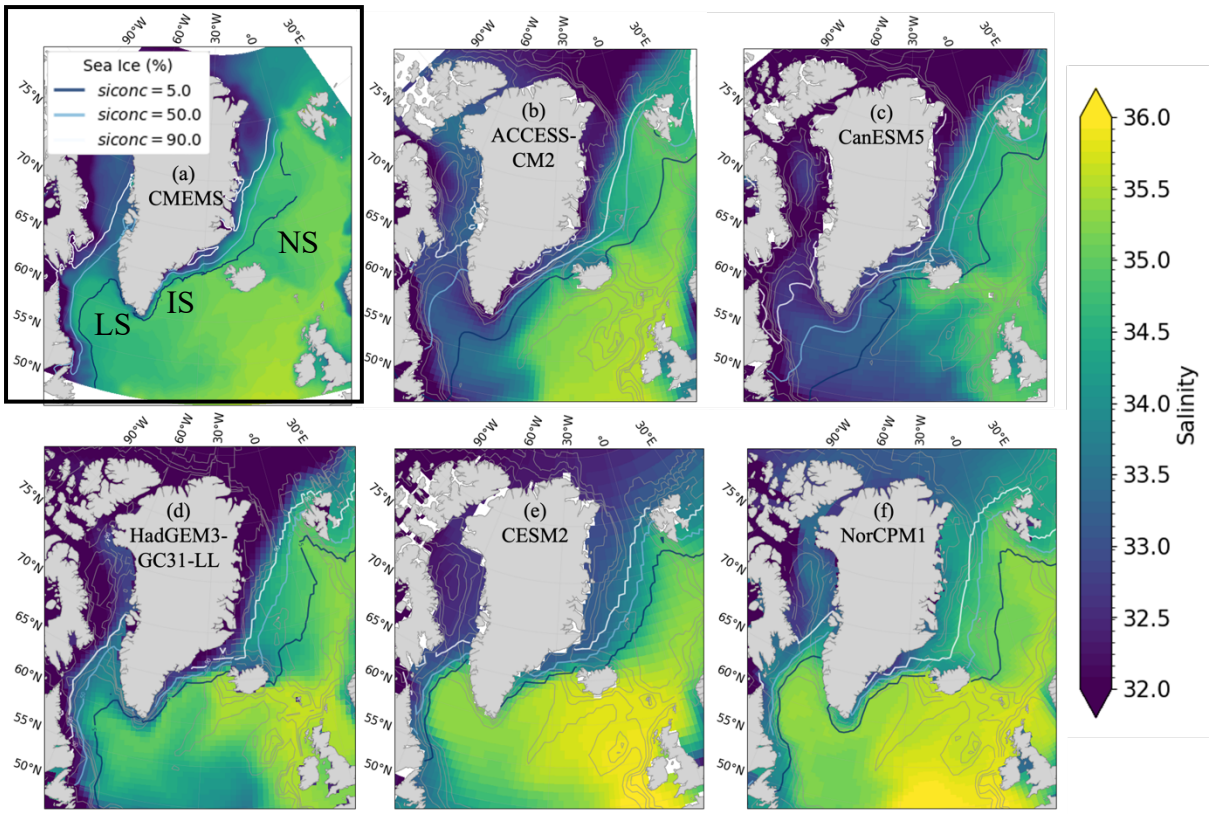

Figure 7: Mean winter (JFM) CMEMS sea surface salinity (SSS) from 1993 to 2014 with labelled LS: Labrador Sea, IS: Irminger Sea, NS: Nordic Seas, b-f) Model mean winter (JFM) 1993 - 2014 SSS. Salinity is between 32 (freshest) and 36 (most saline). Sea ice concentration is shown as contour lines for 5, 50 and 90 %, indicating the percentage of the grid cell covered by ice. Isobaths in grey at 200, 500, 1000, 2000, 5000 m.

Salinity plays a large role in the density stratification of the water, and thus the potential for deep mixing, and is important to represent accurately in climate models. Salinity can be affected by the presence of sea ice, which acts to lower the salinity and increase the buoyancy.

Throughout the lower east SPNA, the mean SSS for the reanalysis (Fig. 7a) and models (Fig. 7b-f) is saltier than the fresher upper west SPNA. The spatial pattern of salinity varies significantly between models. For example, CESM2 (Fig. 7e) and NorCPM1 (Fig. 7f) show the saltiest SPNA ocean, with a salinity of up to 36 near the UK. These two models have a positive salinity bias throughout the SPNA compared to the reanalysis and the rest of the models, with low sea ice concentrations, especially in the Labrador Sea. Note, these models had the highest AMOC strengths, contributing to the higher salinity transport into the SPNA (see Figure 4). ACCESS-CM2 (Fig. 7b) and CanESM5 (Fig. 7c) have a significant freshwater bias with high concentrations of sea ice in the Labrador Sea compared to the reanalysis and the rest of the models. CanESM5 has the lowest AMOC strength out of all the models and has the lowest salinity throughout the SPNA with an overestimation of sea ice concentration (> 50 %), especially in the Labrador Sea and extending into the North Atlantic. HadGEM3-GC31-LL (Fig. 7d) has a relatively fresh bias throughout the lower SPNA and Nordic Seas but overall compares best to the CMEMS also in terms of sea ice concentrations (Fig. 7a).

In the SPNA, water mass properties are often density-compensating. The East Greenland Current (EGC) is cold and fresh, while the North Atlantic Current (NAC) is warm and saline. Therefore, we have to investigate their combined effect on the stratification and how this affects the location and depth of mixed layers for deep convection. For cold temperatures, the salinity plays a larger role in determining the density of the water, and thus salinity changes can be more significant than temperature changes for stratification in this region. If the waters are too strongly stratified (with lighter layers on top of denser layers) due to fresh or warm water, then no mixing can occur.

By calculating the buoyancy (see Equation 1, Section 2.3) of the upper 500 m, regions with higher buoyancy (higher stratification) can be identified. Due to the regridding of the hydrographic sections, some irregularities may be seen in the hydrographic plots, especially towards the east Greenland coast, and should be taken into consideration. First, the buoyancy for the summer months is shown when the waters have restratified after the deep convection of the previous winter if deep convection has occurred. High buoyancy is seen year-round for regions where no deep convection occurs, such as in the Arctic (very cold but fresh waters). Higher temperatures in the east SPNA also cause higher buoyancy during the summer. For the winter months, regions of zero buoyancy indicate potential convection regions.

8.1 Summer (JAS)

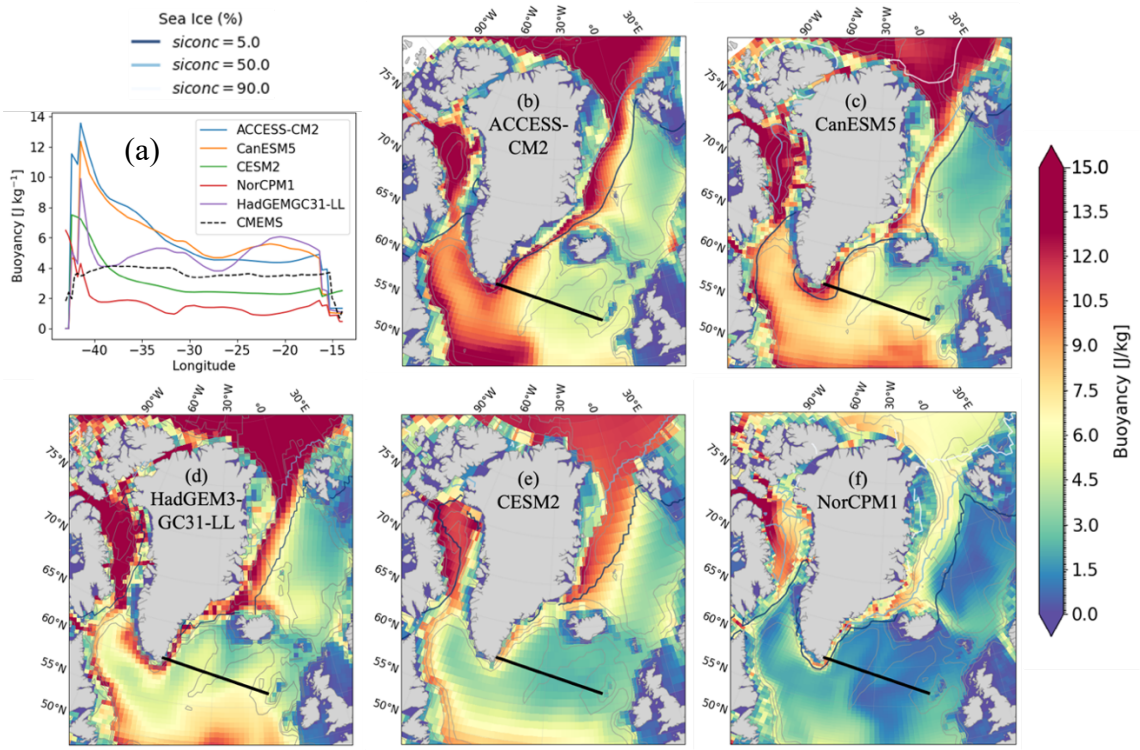

8.2 Winter (JFM)

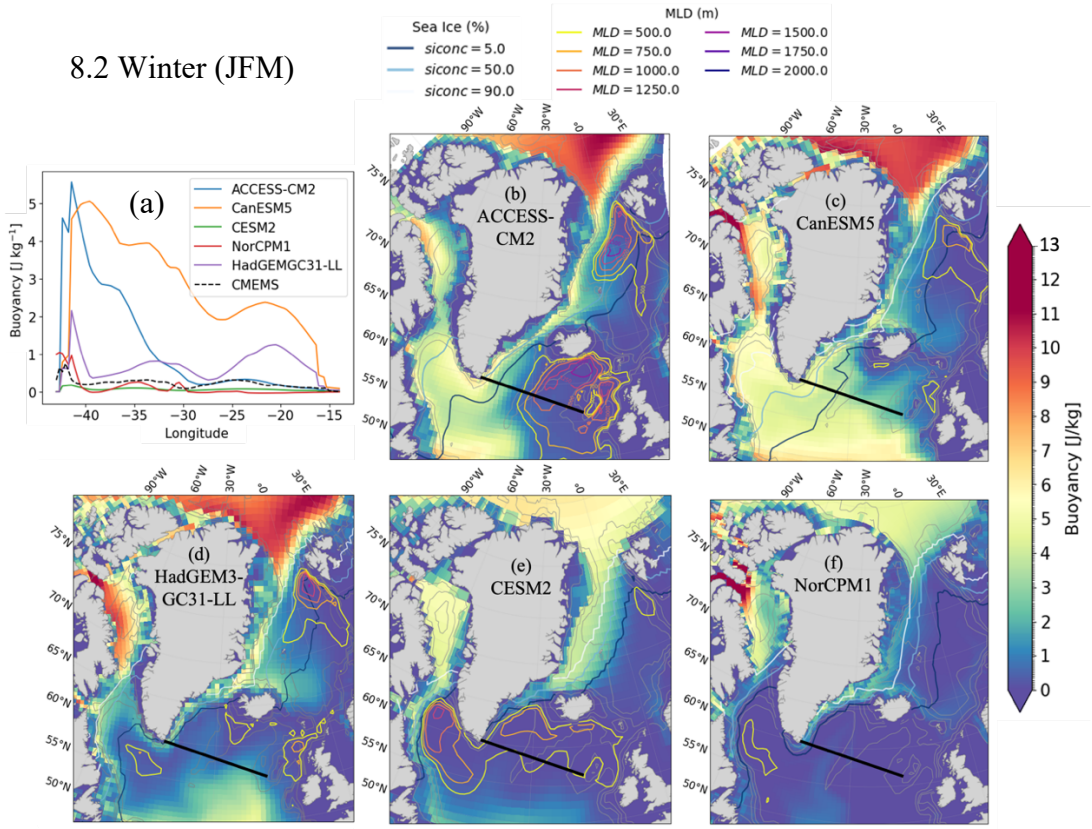

Figure 8: Mean summer (JAS) model buoyancy (J/kg) in the upper 500 m from 1993 to 2014 for 8.1(a) CMEMS (dashed black lines) and all models (coloured lines) and 8.1(b-f) model buoyancy upper 500m. 8.2(a) winter (JFM) CMEMS (black dashed line) and all models (coloured lines), (b-f) Model mean winter (JFM) 1993 - 2014 buoyancy (J/kg) for the upper 500 m with mixed layer depth contours of 500, 750, 1000, 1250, 1500 m from yellow to red. Sea ice concentration is shown as contour lines for 5, 50 and 90 %, indicating the percentage of the grid cell covered by ice. Isobaths in grey at 200, 500, 1000, 2000, 5000 m. Black lines on all maps indicate the hydrographic section, shown in Figure (a).

In the summer, warmer temperatures and more (fresh) meltwater from the Arctic sea ice or Greenland ice sheet increase the buoyancy of the water in the SPNA. For the summer (JAS) buoyancy in Figure 8.1, most models show very high stratification throughout the SPNA, especially in the Arctic and Labrador Sea for ACCESS-CM2 (Fig. 8.1b) and CanESM5 (Fig. 8.2c). NorCPM1 (Fig. 8.1f) has the lowest buoyancy throughout the SPNA of all the models. All models show very high buoyancy in the Arctic Sea and especially in the Labrador Sea, with regions of higher buoyancy around Greenland where fresh meltwater is present.

In the winter, surface cooling and reduced melting lower the buoyancy of the water, allowing for deep convection in regions of zero buoyancy with sufficient surface forcing by winds. In Figure 8.2a, buoyancy is highest in two models, the ACCESS-CM2 (blue line) and CanESM5 (orange line). This is also seen in the higher buoyancy from the east Greenland shelf in Figures 8.2b and 8.2c, respectively A high buoyancy corresponds to high stratification, and thus less potential for mixing. CESM2 (Fig. 8e) and NorCPM1 (Fig. 8f) have the lowest buoyancy in the Labrador Sea and throughout the SPNA, with even the Arctic Sea showing relatively low values compared to the other three models. The mixed layer depth (MLD) contour lines (deeper than 500 m) in Figure 8.2(b-f) show regions of deep convection. ACCESS-CM2 (Fig. 8.2b) shows the deepest MLD in the regions of zero buoyancy of the Iceland Basin and Nordic Seas, but the Labrador Sea is too stratified due to the presence of sea ice decreasing the salinity of the water and preventing surface heat loss. For the other models, even where the buoyancy is zero, the MLD is not deep. This is especially the case for NorCPM1 (Fig. 8.2f) which shows the shallowest MLD, only down to 500 m in the Labrador Sea, and does not convect significantly in other regions of the SPNA despite the low stratification. In NorCPM1, the buoyancy is low in the summer, and no significant buoyancy loss occurs before the winter, necessary to initiate the process of deep convection. This could be due to reduced air-sea exchange in the region.

The mixed layer depth was shown already in Figure 8.2 as contour lines on the stratification and compared to the hydrographic section of buoyancy for CMEMS. To get a better understanding of where mixing occurs, the MLD is shown in Figure 9, indicating regions of deep convection, and highlighting differences between the models and reanalysis. The mean of the mixed layer depth is shown for the winter months (JFM) from 1993 – 2014, with the sea ice concentration as contour lines. Note, the maximum depths can be much deeper and can vary significantly from year to year.

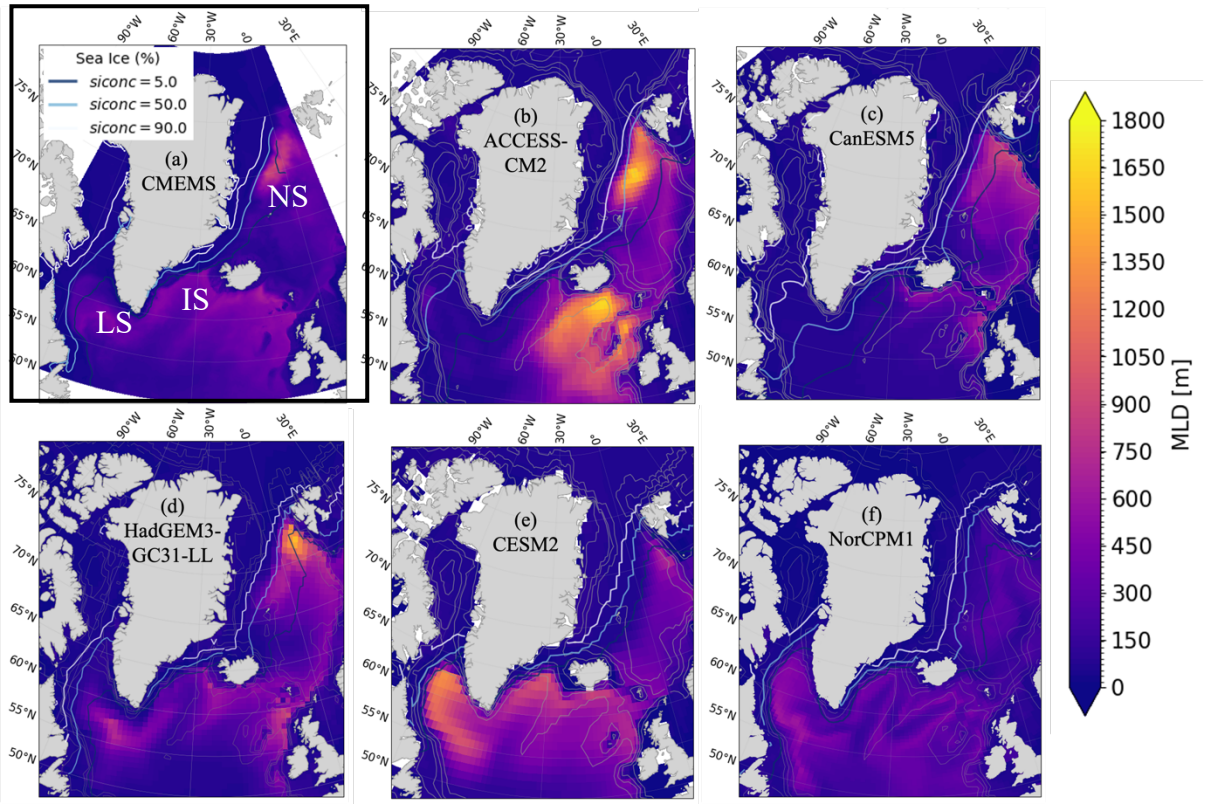

Figure 9: a) Mean winter (JFM) CMEMS mixed layer depth (MLD, m) from 1993 to 2014 with labelled LS: Labrador Sea, IS: Irminger Sea, NS: Nordic Seas. b-f) Model mean winter (JFM) 1993 - 2014 MLD (m). Mean MLD values are between 0 and 1800 m. Sea ice concentration is shown as contour lines for 5, 50 and 90 %, indicating the percentage of the grid cell covered by ice. Isobaths in grey at 200, 500, 1000, 2000, 5000 m.

The location of deep convection depends on the stratification and surface fluxes, with deep mixed layers in the Labrador and Irminger Seas preconditioned by the subpolar gyre circulation and strong wind events, as well as in the Nordic Seas at the sea ice edge. For ACCESS-CM2 (Fig. 9b), CanESM5 (Fig. 9c), and HadGEM3-GC31-LL (Fig. 9d), the deepest convection region is in the Nordic Seas, with mean depth beyond 1500 m for ACCESS-CM2. This region of deep convection (NS) occurs adjacent to high concentrations of sea ice (> 50 %) for all three models and the reanalysis (Fig. 9a). For ACCESS-CM2, CanESM5, and HadGEM3-GC31-LL, there is also a mixed layer depth below Iceland (strongest in ACCESS-CM2), but no convection in the Irminger Sea or Labrador Sea for the ACCESS-CM2 and CanESM5. For CESM2 (Fig. 9e) and NorCPM1 (Fig. 9f), the mixed layer depth is deepest in the Labrador Sea (maximum depths > 1200 m for CESM2), extending throughout the SPNA at relatively shallow depths. CMEMS (Fig. 9a) also shows an extensive (but not very deep) mixed layer depth below Iceland and in the Labrador Sea. The shallowest MLD is present in NorCPM1 (maximum depth of 600 m) but is dispersed throughout the SPNA. Overall, the HadGEM3-GC31-LL most closely resembles the spatial pattern of CMEMS for mixed layer depths in the SPNA.

3.2 Hydrographic Sections

Studying surface variables is important for air-sea interactions and buoyancy losses. To get a better representation of the water column stratification and differences between models below the surface, a vertical section is shown across the Irminger and Iceland Basins with potential temperature in Figure 10.

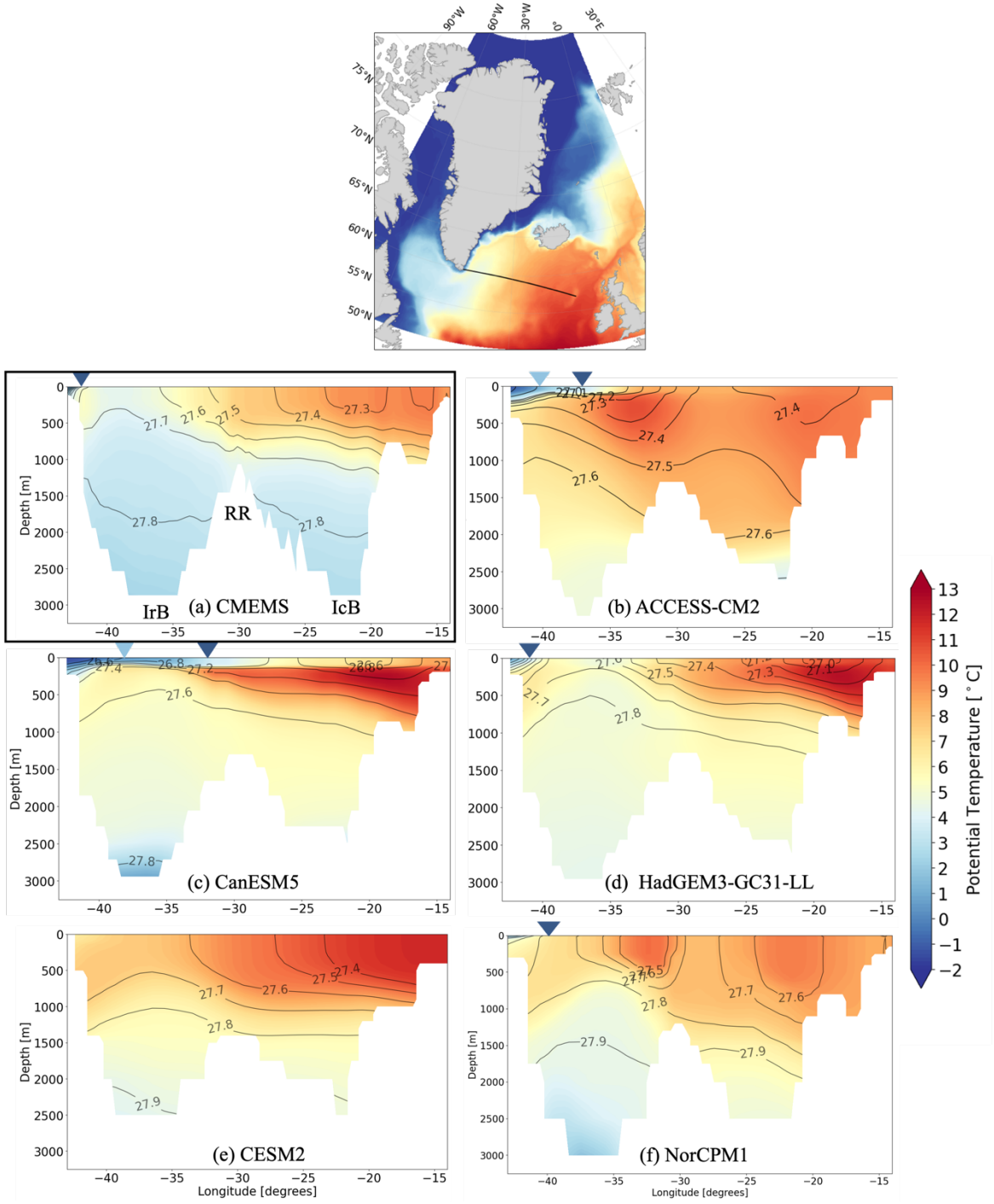

Figure 10: Top figure showing the location of the hydrographic line section on CMEMS SST. Hydrographic mean winter (JFM) potential temperature (°C) from 1993 - 2014 for (a) CMEMS with labelled IrB: Irminger Basin, RR: Reykjanes Ridge and IcB: Iceland Basin, (b-f) CMIP6 models. Isopycnals at 0.1 intervals are shown in black contour lines. Blue triangles show sea ice concentration, increasing towards the east from 5 % in dark blue to 50 % in light blue.

Across this hydrographic section, warm (and saline) NAC waters and the Irminger Current flow northwards, with a return flow near Greenland adjacent to the EGC. Dense bottom waters should be present in the Irminger Basin, overflowing from Denmark Strait. All models and reanalysis in Figure 10 show relatively warm surface layers in the east of the section, with cooler temperatures at depth and in the west (towards Greenland). All models are biased warm across the section compared to CMEMS (Fig. 10a), except for the cold water layer extending from the east Greenland shelf, which is either over-estimated such as in ACCESS-CM2 (Fig. 10b) and CanESM5 (Fig. 10c), not distinct such as in NorCPM1 (Fig. 10f) or not present at all such as in CESM2 (Fig. 10e) with no sea ice on the section. Doming isopycnals are indicative of mixing, with more homogeneous water column properties.

The warmest temperatures of all the models and reanalysis in Figure 10 are in CanESM5 (Fig. 10c) and HadGEM3-GC31-LL (Fig. 10d) at the subsurface layer (up to 13 °C), with a cold surface layer extending from the east Greenland shelf over the Reykjanes Ridge (RR). This is surprising as CanESM5 has the weakest AMOC (see Figure 4), with the lowest sea surface temperatures (see Figure 6). CanESM5 also shows the coldest bottom waters in the Irminger Basin (IrB). The lowest NAC temperatures are in NorCPM1 (Fig. 10f) despite its high AMOC strength (see Figure 4), although a large warm extent is observed in the top 1500 m, with the EGC barely visible in the top left corner. NorCPM1 also has colder waters extending down from ~ 500 m to the bottom of the Irminger Basin, with doming isopycnals here. ACCESS-CM2 (Fig. 10b) has the deepest warm water extent throughout the section. The sea ice contours (triangles on top of model figures) show the extent of the sea ice on the surface of the water and lower temperatures beneath. The model that most closely resembles the spatial pattern of CMEMS (Fig. 10a) is HadGEM3-GC31-LL (Fig. 10f) albeit with a warm bias across the section.

The practical salinity across the same hydrographic section is shown in Figure 11, with the line first shown on top of the CMEMS winter (JFM) SSS for reference.

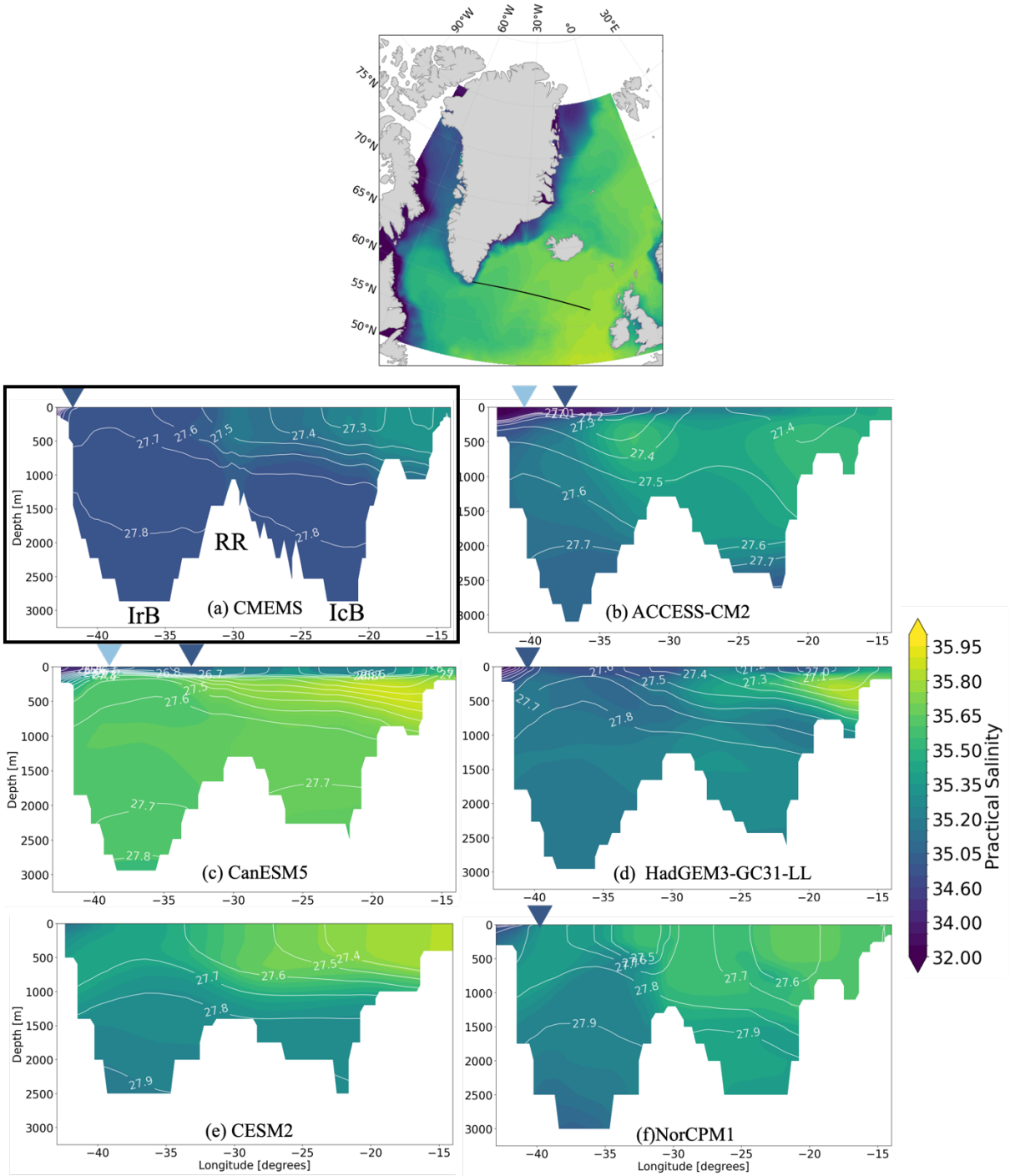

Figure 11: Top figure showing the location of the hydrographic section on top of CMEMS winter (JFM) sea surface salinity (SSS). Hydrographic mean winter (JFM) practical salinity from 1993 – 2014 for (a) CMEMS with labelled IrB: Irminger Basin, RR: Reykjanes Ridge and IcB: Iceland Basin, and for (b-f) CMIP6 models. The salinity scale ranges from 32 (freshest) to 36 (most saline) and is not uniformly spaced. Isopycnals at 0.2 or 0.1 intervals are shown in white contour lines. Blue triangles show sea ice concentration, increasing towards the east from 5 % in dark blue to 50 % in light blue.

Saline waters enter the SPNA through the NAC, flowing into the Irminger Sea through the Irminger Current and entering the Labrador Sea. In Figure 11, most models show the highest salinities towards the east of the section, associated with more saline waters in the NAC. Freshwater is located near the surface at the east Greenland shelf, with varying salinities and extensions towards the bottom of the Irminger Basin (IrB) throughout the models. CanESM5 (Fig. 11c) shows the freshest and most extensive surface freshwater layer across the section for all models. This layer extends throughout the upper 100 – 200 m and is most fresh near east Greenland. However, the rest of the basin is biased saline in comparison to CMEMS (Fig. 11a). ACCESS-CM2 (Fig. 11b) also shows an extensive freshwater layer on the surface from east Greenland towards the Reykjanes Ridge, with high sea ice concentrations. HadGEM3-GC31-LL (Fig. 11d) shows a more localized freshwater region towards east Greenland and relatively homogeneous and fresh waters throughout the basin but with a saltier region in the east subsurface waters. CESM2 (Fig. 11e) and NorCPM1 (Fig. 11f) show a very slight decrease in salinity in the location of the EGC, but not to a significant extent, and are mostly biased salty throughout the basin compared to CMEMS. Most models are relatively homogeneous in the lower depths of the section, with the most variability of freshwaters in the upper 500 m.

With the previous results of temperature and salinity and corresponding isopycnals, we can say which models are too dense (HadGEM3-GC31-LL and NorCPM1), too light (ACCESS-CM2, CanESM5), and which show the least bias compared to reanalysis in terms of density (CESM2). From previous results of buoyancy (stratification), we showed that, for the winter months, NorCPM1 had very low buoyancy (low stratification) in the upper 500 m as seen by the vertically sloping isopycnals. ACCESS-CM2 and CanESM5 showed the highest buoyancy across the hydrographic section, which shows relatively stratified layers from the isopycnals. HadGEM3-GC31-LL shows relatively stratified layers (more towards the east, in the Iceland Basin), with a doming effect in the Irminger Basin (IrB) indicative of mixing.

To study the movement of currents in this region, transporting heat and salinity, the meridional component of the velocity is shown in the same hydrographic section in Figure 12. Here, only the variable ‘vo’ is used, and so does not represent the perpendicular velocity to the line, but only the northward velocity component. As the hydrographic line section follows quite closely the latitude line (between 58 and 60 °N), this is not deemed to be an issue, and can be considered as waters flowing northwards (positive red values) and southwards (negative blue

values). Note that for NorCPM1 no 'vo' historical variable is available, but the values from 2015 – 2029 are shown instead to determine the behaviour of the model.

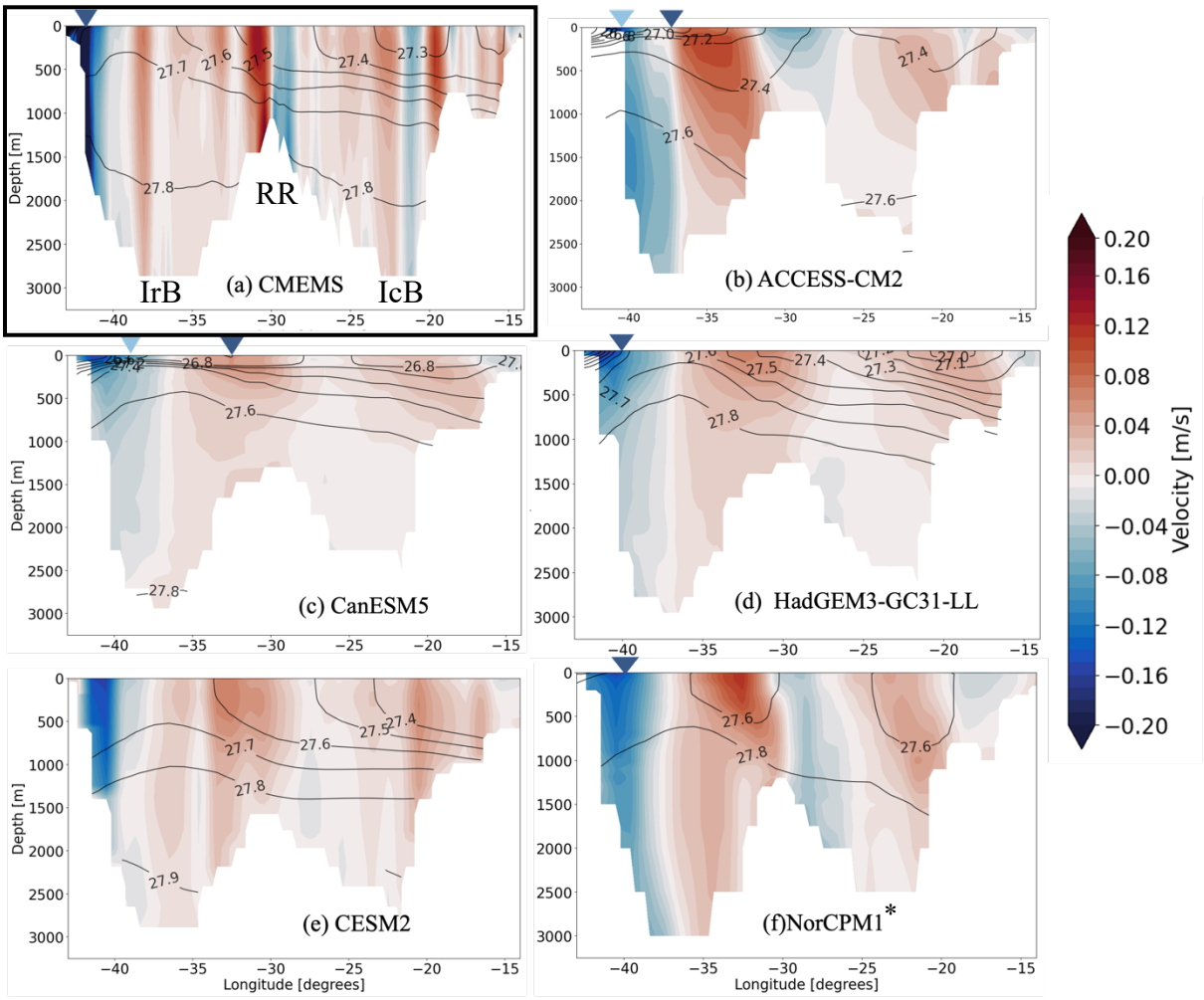

*Figure 12: Hydrographic mean winter (JFM) meridional velocity from 1993 - 2014 for (a) CMEMS with labelled IrB: Irminger Basin, RR: Reykjanes Ridge and IcB: Iceland Basin, and for (b-f) CMIP6 models. The colour scale is from -0.2 to 0.2 m/s. Isopycnals at 0.2 or 0.1 intervals are shown as black contour lines. *NorCPM1 did not provide historical dates for the 'vo' variable, but the dates from 2015 – 2029 are shown. Blue triangles show sea ice concentration, increasing towards the east from 5 % in dark blue to 50 % in light blue.*

The representation of circulation in models is important for the transport of heat, and salinity, especially here in the SPNA with regions of deep convection. Figure 12 shows most water across the section flowing northward (red colour) for all models and CMEMS, with currents extending from the surface to the bottom of the basins across the section. The velocities are all slower and wider in the models (Fig. 12b-f) than in CMEMS (Fig. 12a). Most models show weak but deep northward currents throughout the basin and a stronger, more localized southward flow in the Irminger Basin. CESM2 (Fig. 12e) shows the strongest southward flowing water near east Greenland for the models (maximum speed –0.18 m s^{-1}), while for the other models, this current (blue southward flow next to east Greenland) is deeper and slower,

with highest velocities at the surface. NorCPM1 (Fig. 12f) has the fastest meridional velocity, with the highest northward flow over the west RR. For CanESM5 (Fig. 12c) and HadGEM3-GC31-LL (Fig. 12d), the southward flowing currents near the east Greenland shelf are fastest at the surface but extend down to (almost) the bottom of the basin. Overall, none of the models are able to represent the circulation as in CMEMS, due to their coarser ocean resolution. In CMEMS, distinct north and southward flows are present on the Reykjanes Ridge, with ACCESS-CM2 most closely resembling this spatial pattern (also NorCPM1 but not for historical data).

In the next section, one model is compared at different ocean resolution. From the previous results, it has been shown that the models present biases in the SPNA for temperature and salinity, mostly in the Labrador Sea with varying sea ice concentrations impacting the salinity and temperature and hence the density of the water in this region. Accurate representation of the location and intensity of currents are important in a model, as they determine the amount of heat or salt transported to certain regions. If these smaller-scale processes are not resolved, this can lead to further biases in low-resolution models. By analysing how a higher resolution model performs, again in comparison to the reanalysis, we can see if increasing the resolution improves this representation of circulation in the Subpolar North Atlantic and associated processes with deep convection.

3.3 HadGEM-GC31 Low (-LL) and Medium (-MM) Resolution

In this section, two different resolutions for the HadGEM3-GC31 model are analysed and compared to CMEMS reanalysis in terms of stratification and deep convection. HadGEM3-GC31-LL has a low (L) ocean resolution of 100 km, and a low (L) atmospheric resolution of 250 km, HadGEM3-GC31-MM has a medium (M) ocean horizontal resolution of 25 km, and a medium (M) atmospheric horizontal resolution of 100 km. Details of these models can be found in Section 2.1, Table 1.

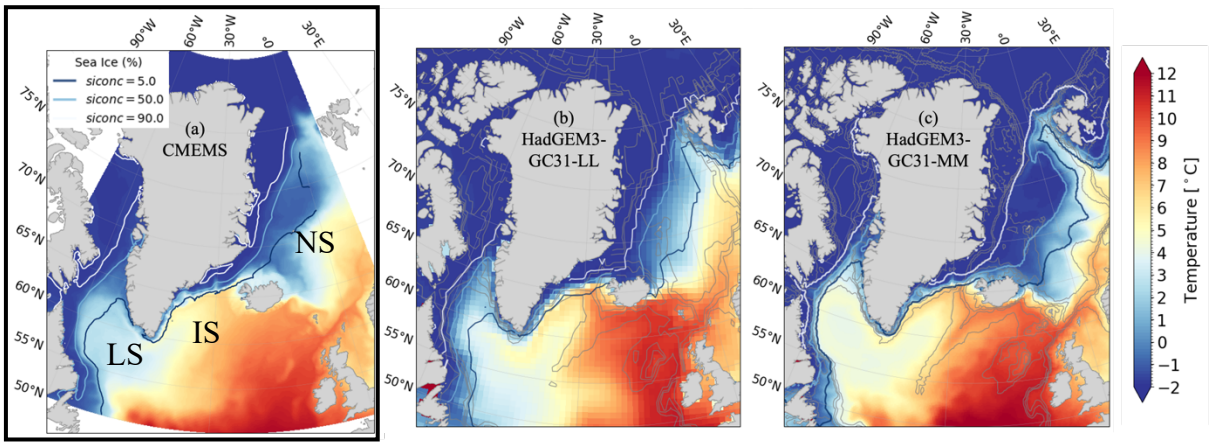

Figure 13: Mean winter (JFM) sea surface temperature (°C) from 1993 – 2014 for (a) CMEMS with labelled LS: Labrador Sea, IS: Irminger Sea, NS: Nordic Seas, (b) HadGEM3-GC31-LL (low resolution) and (b) HadGEM3-GC31-MM (medium resolution). Temperatures are between -2 and 12 °C. Sea ice concentration is shown as contour lines for 5, 50 and 90 %, indicating the percentage of the grid cell covered by ice. Isobaths in grey at 200, 500, 1000, 2000, 5000 m.

At higher resolution, smaller-scale currents and processes can be represented in a model, instead of being parametrized. In Figure 13, both HadGEM3-GC31 models show similar patterns of sea surface temperature in the SPNA. The influx of warm surface waters from the NAC in the lower east SPNA extends northwards to the Nordic Seas and westward into the Irminger and Labrador Seas. Cold temperatures extend from the Arctic, following the coast of Greenland. The North Atlantic Corner (warm current in lower west SPNA near Canada) is visible only in MM and is comparable to CMEMS, while for the lower resolution model, this feature is not resolved. The sea ice extent is similar for 90 percentile contours in both models, but the 50 and 5 percentile contours extend further in the Nordic Seas for MM (Fig. 13c), and further in the Labrador Sea for LL (Fig. 13b) with lower sea surface temperatures. HadGEM3-GC31-MM is biased warm by a few degrees in the Labrador Sea compared to CMEMS, with LL showing temperatures comparable to CMEMS with a slightly enhanced warm current entering the Labrador Sea. Both models are able to resolve the Irminger Current, warm waters extending from the NAC, flowing around the Irminger Sea and into the Labrador Sea.

These spatial patterns of warm or cold currents are expected to be similar in the sea surface salinity. Here, the sea surface practical salinities are compared in Figure 14.

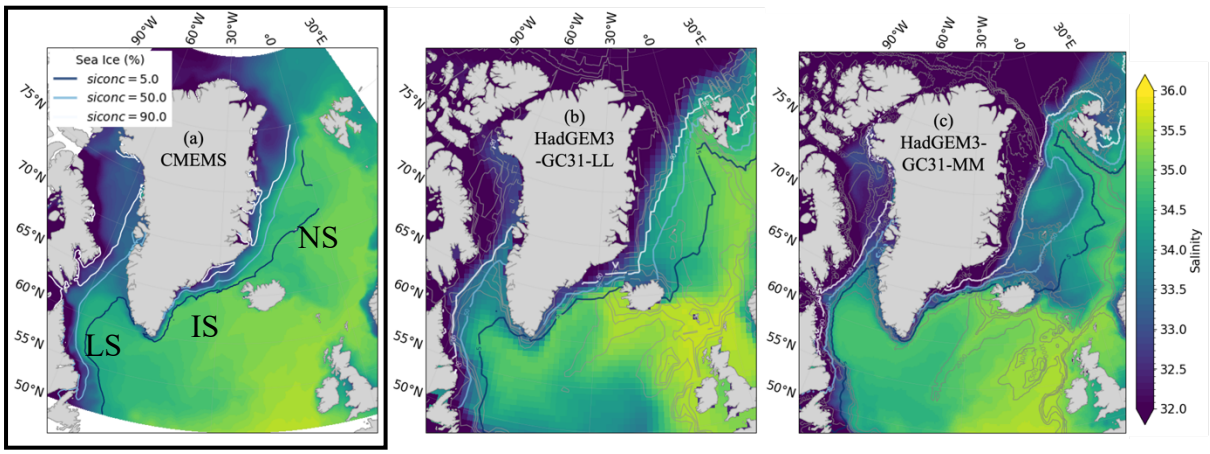

Figure 14: Mean winter (JFM) sea surface salinity (SSS) from 1993 to 2014 with labelled LS: Labrador Sea, IS: Irminger Sea, NS: Nordic Seas for (a) CMEMS, (b) HadGEM3-GC31-LL (low resolution), (c) HadGEM3-GC31-MM (medium resolution). Salinity is between 32 (freshest) and 36 (most saline). Sea ice concentration is shown as contour lines for 5, 50 and 90 %, indicating the percentage of the grid cell covered by ice. Isobaths in grey at 200, 500, 1000, 2000, 5000 m.

Fresh Arctic water lowers the salinity in the north SPNA, extending around Greenland and into the Labrador Sea via the East Greenland Current. Salty water enters the SPNA from the NAC, with the strength of the AMOC influencing the salt transport (not directly shown here). The low-resolution model (LL, Fig. 14b) shows the highest salinities in the west SPNA, especially below Iceland and close to the UK, extending into the Nordic Seas. In the medium resolution model (MM, Fig. 14c), the salinity in the lower SPNA is comparable to the CMEMS (Fig. 14a), but is considerably lower in the Nordic Seas, with a high sea ice concentration biasing the salinity northwards of Iceland. The freshwater around Greenland is confined closer to the coast for the MM compared to LL, in better agreement with CMEMS. The North Atlantic is biased fresh for LL, with relatively high sea ice concentrations in the Labrador Sea and lower salinity. Overall, both models show biases in the representation of salinity throughout the SPNA, with no significant improvement for the higher-resolution model compared to the lower resolution.

Next, we show the buoyancy, calculated from the above salinity and temperatures to show the stratification differences between the two resolutions and the reanalysis. First, the comparison to CMEMS across the hydrographic section is shown, then the two maps for LL and MM of buoyancy with sea ice concentration and mixed layer depth (deeper than 500 m) are shown. The buoyancy for the summer months is shown in Appendix 1.2, Figure 27, showing similar high buoyancies throughout the SPNA for both models.

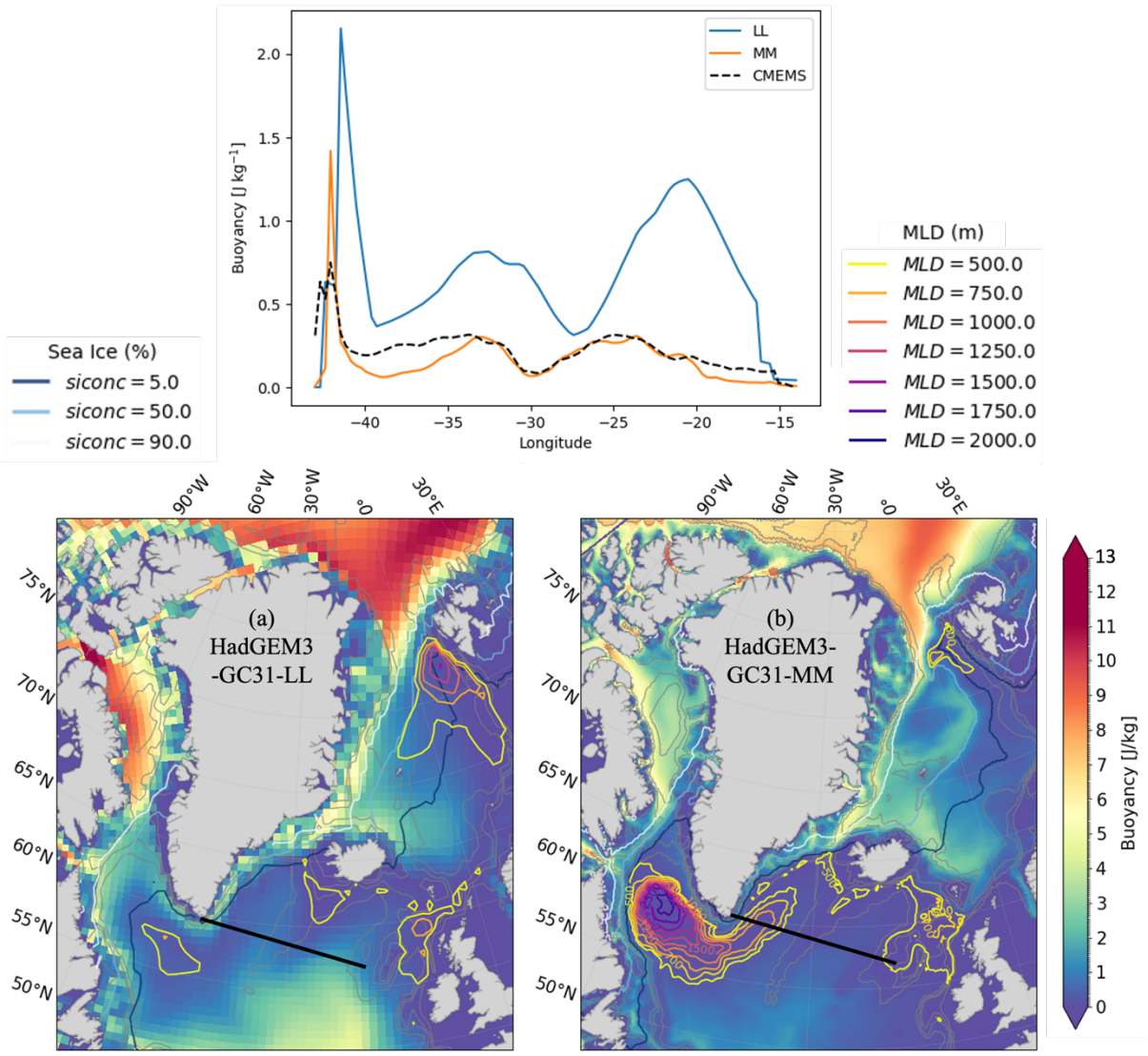

Figure 15: Top figure shows the mean winter (JFM) buoyancy (J/kg) in the upper 500 m from 1993 to 2014 for both resolutions of HadGEM3-GC31 (LL blue and MM orange line) and CMEMS (dashed black line) across the hydrographic section (black lines in figures below. (a) HadGEM3-GC31-LL (low resolution) and (b) HadGEM3-GC31-MM (medium resolution) model mean winter (JFM) 1993 - 2014 buoyancy (J/kg) for the upper 500 m. Buoyancy values are between 0 (no stratification) and 13 J/kg (highest stratification). Mixed layer depth is shown by the yellow to red contour lines from 500 to 2500 m with 250 m spacing. Sea ice concentration is shown as contour lines for 5, 50 and 90 %, indicating the percentage of the grid cell covered by ice. Isobaths in grey at 200, 500, 1000, 2000, 5000 m.

Even though differences between the two model resolutions were not extreme for the temperature and salinity, the stratification and consequent deep convection can vary significantly depending on the surface forcings and representation of mixing within each model. The top panel in Figure 15 shows the winter (JFM) buoyancy summed over the top 500 m across the hydrographic section for both LL (Fig. 15a) and MM (Fig. 15b). This shows LL as having a higher buoyancy overall compared to MM across the section, which compares relatively well with the CMEMS section. In Figures 15a and b, the spatial pattern of buoyancy is similar, with LL showing higher buoyancy in the Labrador Sea and throughout the North Atlantic, as well as much higher values in the Arctic (~ 12 J kg^{-1}). Meanwhile, MM has little

to no buoyancy throughout the lower SPNA but is slightly higher in the Nordic Seas just above Iceland where the sea ice concentration (> 5 %) is higher compared to LL. These patterns of buoyancy can indicate where mixing and deep convection occurs.

Mixed layers deeper than 500 m are not present in all regions of zero buoyancy for either model in Figure 15. The zero buoyancy in the Labrador Sea for MM allows for very deep convection unrealistic depths, while for LL, most of the deep convection occurs in the Nordic Seas near the sea ice edge of 50 % concentration. The mixed layer depth for the two resolutions of HadGEM3-GC31 is compared in more detail also to the CMEMS reanalysis in Figure 16.

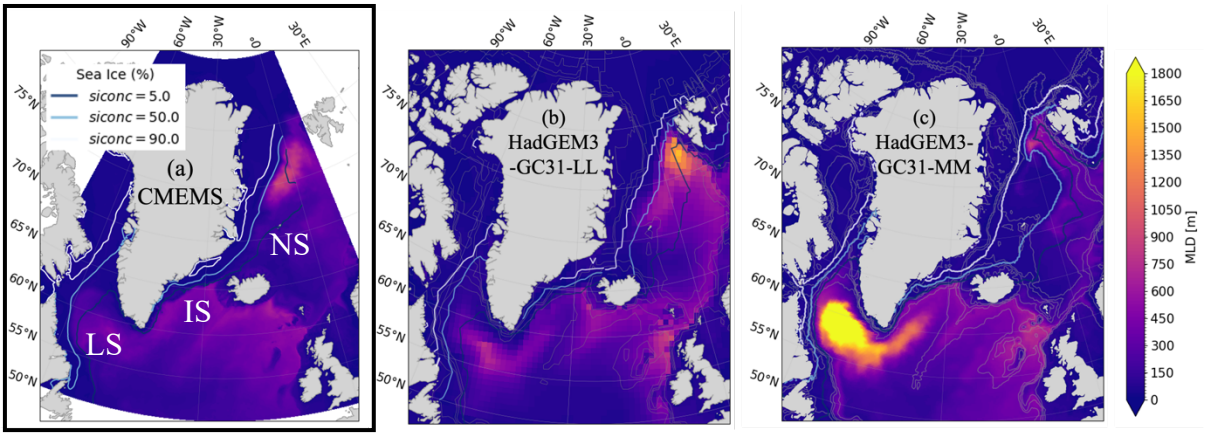

Figure 16: Mean winter (JFM) mixed layer depth (MLD, m) from 1993 to 2014 with labelled LS: Labrador Sea, IS: Irminger Sea, NS: Nordic Seas for (a) CMEMS, (b) HadGEM3-GC31-LL (low resolution) and (c) HadGEM3-GC31-MM (medium resolution). Mean MLD values are between 0 m (no mixing) and 1800 m (deep convection). Sea ice concentration is shown as contour lines for 5, 50 and 90 %, indicating the percentage of the grid cell covered by ice. Isobaths are shown in grey at 200, 500, 1000, 2000, 5000 m.

The mixed layer depth (MLD) is very different for the two resolutions of HadGEM3-GC31. For the low resolution (Fig. 16b), the MLD is deepest in the Nordic Seas (with values above 1400 m). For this model, a relatively shallow (~ 800 m) MLD extends throughout the SPNA (Labrador and Irminger Seas), more closely resembling the CMEMS (Fig. 16a). For MM (Fig. 16c), the MLD is deepest in the Labrador Sea (> 1800 m, to the sea floor), and extends into the Irminger Sea. There is no significant mixed layer depth in the Nordic seas in this MM model. While the LL model more closely resembles the CMEMS product, comparison to Argo data (see Appendix 1.1 Figure 24 and 25) shows that more convection should be present in the Labrador Sea to maximum depths of 2000 m. This convection is seen in MM, with very deep mixed layer depths, but to a very large extent which is not considered realistic.

3.4 Hydrographic Sections for HadGEM3-GC31-LL and -MM

To see differences throughout the water column and potential biases for temperature, salinity, and consequently stratification, we show the hydrographic sections along the same line as Section 3.2. HadGEM3-GC31-LL and HadGEM3-GC31-MM are compared to CMEMS. First, the hydrographic sections for potential temperature are shown with isopycnals as black contour lines showing the stratification across the section in Figure 17.

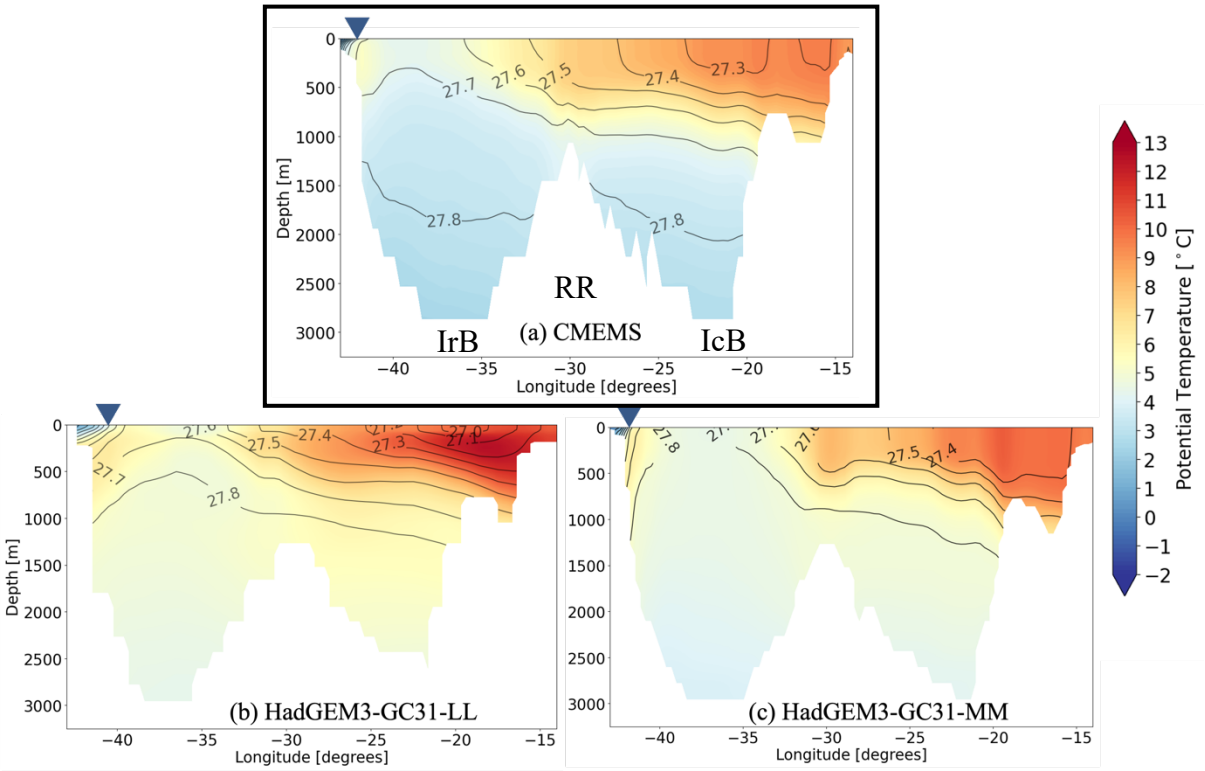

Figure 17: Hydrographic mean winter (JFM) potential temperature (°C) from 1993 - 2014 for (a) CMEMS with labelled IrB: Irminger Basin, RR: Reykjanes Ridge and IcB: Iceland Basin, (b) HadGEM3-GC31-LL (low resolution) and (c) HadGEM3-GC31-MM (medium resolution). Isopycnals at 0.1 intervals are shown in black contour lines. Dark blue triangles indicate a 5 % sea ice concentration, increasing towards the east.

From Figure 17, both model resolutions of HadGEM3-GC31 show a similar pattern for the spatial distribution of potential temperature along the section. Warm North Atlantic waters are present in the top ~ 1000 m in both cases, with LL (Fig. 17b) model showing a higher temperature concentrated in the top right corner, but not at the very surface. Both LL (Fig. 17b) and MM (Fig. 17c) show a cold EGC in the top left corner. LL shows higher stratification than MM and CMEMS, with narrower currents (vertically) and less doming of isopycnals in the Irminger Basin (IrB). The temperatures throughout the Irminger and Iceland Basins (IcB) are slightly lower for the MM model than LL, which has warmer surface temperatures (extending down to 500 m). Both model resolutions show a warm bias (worse in LL) throughout the section compared to CMEMS (Fig. 17a). The EGC is more extended towards the west in LL.

The practical salinity along the section for both models and CMEMS is shown in Figure 18.

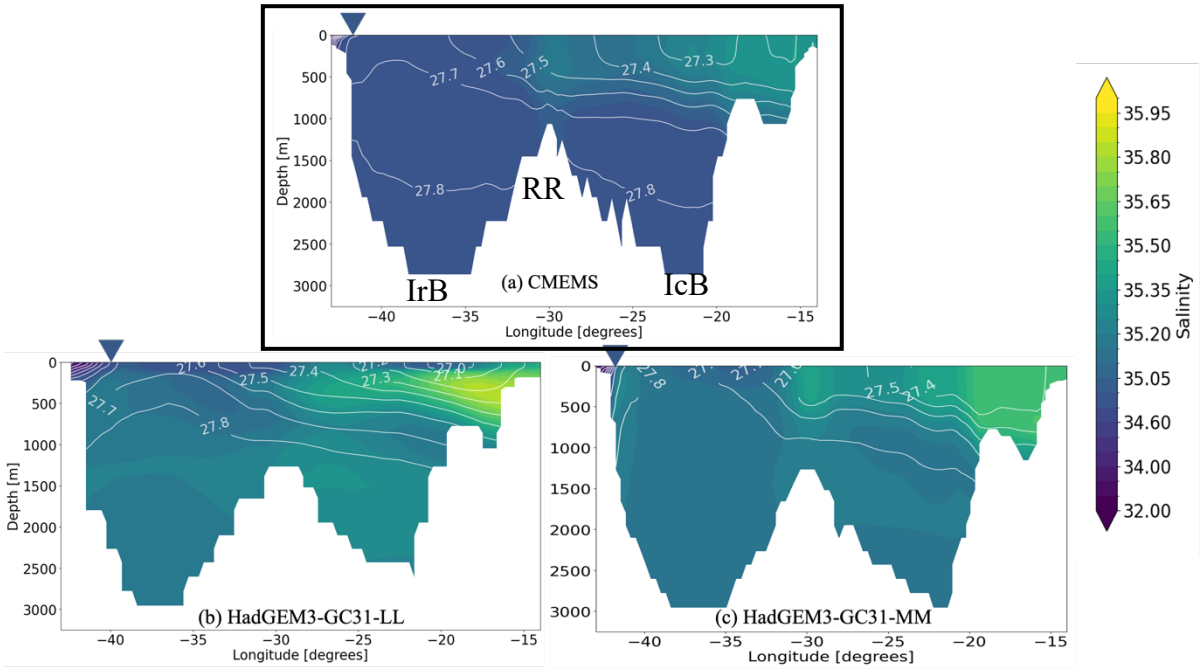

Figure 18: Hydrographic mean winter (JFM) practical salinity from 1993 - 2014 for (a) CMEMS with labelled IrB: Irminger Basin, RR: Reykjanes Ridge and IcB: Iceland Basin, (b) HadGEM3-GC31-LL (low resolution) and (c) HadGEM3-GC31-MM (medium resolution). Isopycnals at 0.2 or 0.1 intervals are shown in black contour lines.

From Figure 18, both models show higher salinities than the CMEMS (Fig. 18a), much higher in LL (Fig. 18b), towards the east in the subsurface (100 – 1000 m). A fresh EGC is present in both models (top left corner), with more extensive fresh surface waters for the LL than the MM model. The salinity is relatively homogeneous throughout the bottom of the basin in both cases. The isopycnals in LL show high stratification throughout the Iceland Basin and steeper isopycnals in the Irminger Basin. Overall, the MM model more closely represents the salinity across the section compared to CMEMS, but the isopycnals in the Irminger Basin are domed and very steep, indicative of mixing, while for the CMEMS the section is more stably stratified. Neither model can be said to better represent the CMEMS salinity across the section.

4 Summary & Discussion

With the results found throughout this work, the research questions stated in Section 1.6 can be answered, providing a summary of the main findings.

4.1 Answering Research Questions

1. *How are winter sea surface temperature and salinity represented?*

All models show a warm surface NAC entering the lower SPNA and extending into the Nordic Seas northeast of Iceland. Higher temperatures entering the lower SPNA can be linked to a stronger AMOC, transporting more warm waters in surface layers. This is connected to the concentrations of sea ice, with weaker AMOC transporting less heat to the SPNA and allowing for more sea ice coverage. However, these two factors are linked, as a higher sea ice concentration can reduce the temperature in the SPNA. AMOC strength is not the only factor in determining the temperature biases in the SPNA, as models with very different AMOC strengths can still have similar SSTs throughout the SPNA, depending on the sea ice and potentially atmospheric factors. This sea ice can decrease the salinity of the water, as regions with lower SSTs and SSSs are covered by sea ice, with major differences between models in the Labrador Sea impacting the location accuracy of deep convection. Models with high SSTs in the lower SPNA also show higher salinities, transported by the stronger NAC. Overall, HadGEM3-GC31-LL was shown to be the least biased compared to CMEMS in terms of sea surface temperatures and salinity.

2. *How do buoyancy differences from summer to winter influence mixed layer depths?*

Higher buoyancy, due to warmer or fresher surface waters, increases the stratification of the water column. If this stratification is not eroded by surface fluxes or increases in density, the potential for mixing and deep convection is reduced, decreasing the strength of the overturning circulation in the SPNA. In the summer, high buoyancy is present throughout the SPNA due to warmer temperatures and more freshwater from the melting of sea ice and runoff from Greenland. In the models, high buoyancy is generally seen in the Arctic Seas and the Labrador Sea. During the winter, cooler atmospheric temperatures allow for more heat loss from the sea surface, increasing the density and thus decreasing the buoyancy. This can also be influenced by higher salinity, further decreasing the buoyancy. Regions with zero buoyancy can experience deep convection in the winter months when the stratification has been eroded. For the winter months, most models show reduced buoyancy throughout the SPNA. Models with

a very high buoyancy in the Labrador Sea in the summer and a reduced but non-zero buoyancy in the winter do not convection in this region, in contrast to observations and reanalysis. One model, NorCPM1, shows the weakest winter mixed layer depths throughout the SPNA, even with zero buoyancy, likely because the buoyancy was already low in the summer and so not enough stratification has been eroded to allow for significant deep convection.

3. *How does resolution impact the model performance in relation to deep convection?*

The increased model resolution for HadGEM3-GC31 from LL to MM does not drastically change surface properties such as temperature and salinity, except perhaps in the Labrador Sea where MM has a warmer bias compared to LL and CMEMS. The largest difference is in the mixed layer depth in the Labrador Sea, extending to over 2500 m in MM but to less than 1000 m in LL. However, CMEMS is not the best comparison in terms of the real ocean for mixed layer depths, as there should be a deep region of convection in the Labrador Sea extending into the Irminger Sea (see Figure 24 for Argo data in the Appendix). While HadGEM3-GC31-LL closely follows the spatial pattern and depths of mixing throughout the SPNA, HadGEM3-GC31-MM shows a much deeper, but over-estimated mixed layer depth in the Labrador Sea, and can thus not be considered an improvement on the representation of deep convection in the SPNA. However, the salinity in MM is comparable to the reanalysis product in the Labrador Sea, while LL shows a slight fresher bias in this region. Even though the salinity and temperature are similar for the two models, the deeper mixed layer depth for MM in the Labrador Sea could be attributed to other processes not studied here, such as mixing by eddies or air-sea fluxes.

In the next section, we consider future AMOC projections for these CMIP6 models.

4.2 Future AMOC Predictions with CMIP6

Deep convection in the Labrador, Irminger and Nordic Seas can influence the strength of the overturning circulation in the North Atlantic and can impact the validity of future AMOC projections if not represented properly in climate models. In the previous sections, we have compared historical data (1993 - 2014) for CMIP6 models with the reanalysis product of CMEMS. This showed which models have the least biases in terms of temperature and salinity, affecting density stratification and regions of deep convection. Reliable models for the future should be able to represent these processes in the SPNA.

In the introduction, Section 1.5, the strength of the overturning at 26 °N for various CMIP6 models from Weijer et al. (2020) was shown. The AMOC strength over the time period of the observational RAPID array shows the range of model AMOC intensities, but how do these same models perform in future predictions of AMOC strength? Weijer et al. (2020) also look at CMIP6 AMOC strength throughout the 21st century, excluding NorCPM1 as the variable for the AMOC stream function is not available. Their results are shown in Figure 19.

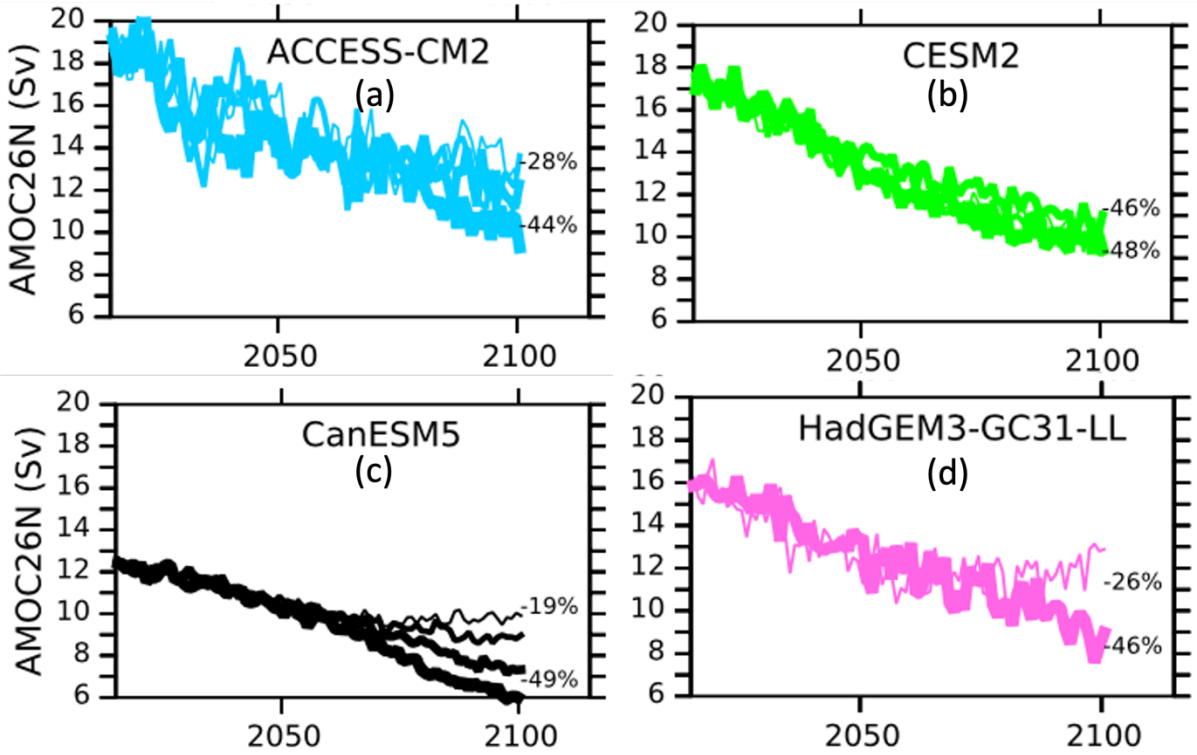

Figure 19: Time series of AMOC at 26N for (a) ACCESS-CM2, (b) CESM2, (c) CanESM5, (d) HadGEM3-GC31-LL. Shown are ensemble means, with progressively thicker lines for the scenarios SSP1-2.6, SSP2-4.5, SSP3-7.0, and SSP5-8.5. Adapted from Weijer et al., (2020).

All models (also the others in Weijer et al., 2020) show a decrease in the AMOC throughout the 21st century for all SSP scenarios. These scenarios range from SSP1-2.5 to SSP5-8.5, depending on the anthropogenic warming compared to pre-industrial levels. More information can be found in IPCC (2022), also showing the multi-model mean decrease for AMOC strength in the 21st century. The largest decrease in the AMOC occurs in the CanESM5 model (-49% for SSP5-8.5, Fig. 19c). This model has the least decrease for the SSP1-2.6 scenario (19 %) with an apparent stabilization in the second half of the 21st century. The weak historical strength of this model produces significant biases in the SPNA for the time period studied in this thesis, resulting in high stratification from freshwater throughout the Labrador and Irminger Seas and no deep convection. These are two important regions of deep convection in the real ocean, and thus this model does not represent SPNA processes realistically.

The least AMOC decline for the highest scenario is by ACCESS-CM2 (Fig. 19a). This model was shown to have relatively low biases of temperature and salinity throughout the SPNA, albeit with a high sea ice concentration in the Labrador Sea causing low salinities and no deep convection. Most of the deep convection for this model occurs in the Nordic Seas and below Iceland, not resembling the spatial pattern or depth from CMEMS. For CESM2, all scenarios share a similar fate, with SSP1-2.6 AMOC declining by 46 % and the SSP5-8.5 scenario decreasing by 48 %. This model was shown to have a high-temperature bias throughout the SPNA, especially in the Labrador Sea, but high salinities allow for dense surface water to mix in this region to mean depths of 1000 m, as well as throughout the Irminger Sea. For HadGEM3-GC31-LL, the AMOC in the SSP1-2.6 scenario decreases by 26 %, but there is a recovery and even strengthening again towards 2100. For the SSP5-8.5 scenario, however, the AMOC decreases by 46 % and shows no sign of recovery. This model was shown to have the least biases overall in SSTs and SSSs compared to CMEMS, however, with relatively weak mixing in the Labrador and Irminger Seas as most of the deep convection occurs in the Nordic Seas.

Important to note is that all high emission scenarios (SSP5-8.5) show a relatively similar decrease in AMOC strength (between 44 and 49 %), but the lower scenarios show much more variability (between 19 and 46 % in the models shown here). This makes future predictions even more uncertain for low emissions scenarios, as there is a large disagreement between the model evolution throughout the 21st century. It cannot be said that if a model performs well with observations, it will also be the most accurate for future projections. However, it can

indicate which models may be more reliable than others, and which are some features of models that should be considered when making predictions such as for the AMOC strength.

Increasing the ocean model resolution for the HadGEM3-GC31 (from LL to MM) did not make a significant difference in terms of sea surface temperature or salinity. However, the mixed layer depth is significantly altered in both location and depth between these two models. Roberts et al. (2019) provide future projections for the AMOC strength for these two models, as well as even higher resolution (HadGEM3-GC31-HH with 10 km ocean resolution), shown in Figure 20.

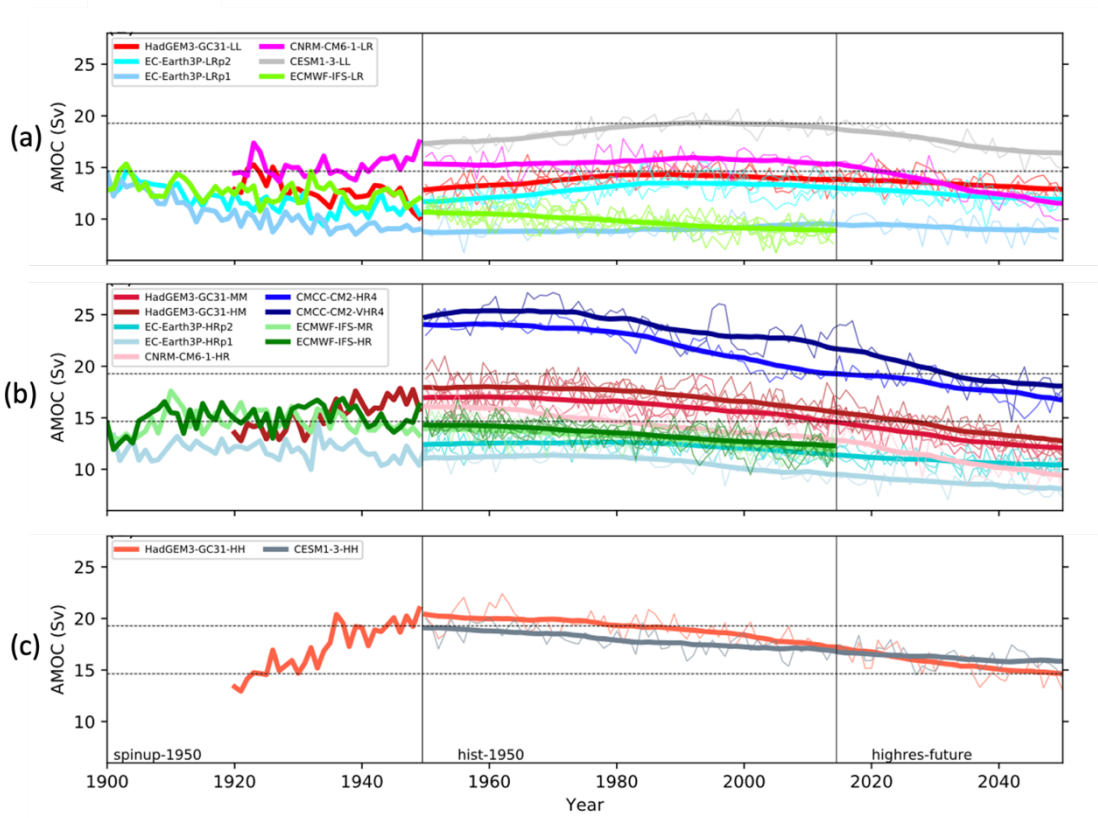

Figure 20: (a-c) Time series of AMOC at 26.5N calculated from spinup-1950, hist-1950 and highres-future-experiments. Each panel shows groups of models with the same ocean resolution, 100, 25 and 8-10 km, respectively. The dashed line indicates the annual mean max/min values from the RAPID-MOCHA array over 2004-2007. Each individual ensemble member is shown as thin lines, apart from the one member spin-up 1950 period shown with thick lines, and the ensemble mean smoothed over a 30 year running mean is shown in bold. Note that all models completed the spinup-1950, but not all the data are available. Adapted from Roberts et al., (2019, their Figure 8).

In their work, Roberts et al. (2019) show that an increased model resolution increases also the strength of the AMOC, tending to agree better with the RAPID-MOCHA observations at 26 °N. However, higher-resolution models also show a very deep or extensive mixed layer depth in the subpolar gyre, not in accordance with observations. Therefore, an increase in resolution from low to medium or even high does not improve behaviour for certain processes such as deep convection, which are important for the evolution of the AMOC. In the future

scenario, they find that high-resolution models tend to show a more rapid decline in the AMOC strength compared to the lower resolution.

As this thesis is focused on historical data (from 1993) we only consider the middle (hist-1950) and right (highres-future) panels in Figure 20 for the following discussion. For HadGEM3-GC31-LL (Fig. 20a) the AMOC is slightly below the RAPID-MOCHA minimum mean (value just below 15 Sv) throughout the historical period and does not show a decrease from its initial value throughout the 21st century. This is different from the behaviour of the MM (Fig. 20b) model in the middle panel, showing a mean AMOC between the maximum and minimum RAPID-MOCHA bounds (at ~ 17 Sv) from the start of the historical period, and decreasing towards 2014 until it reaches the minimum observational mean at just below 15 Sv. An even higher resolution, shown in panel (c), shows that the HadGEM3-GC31-HH (Fig. 20c) starts the historical period above the observational maximum, and decreases towards 2014, where it lies in the middle of the observational range. Both LL and MM models were found to compare relatively well to CMEMS, with MM having a slight cold bias in the Labrador Sea. With higher salinity, however, the MM buoyancy in this region is lower than for LL, which shows a freshwater bias. For the Nordic Seas, the sea ice concentrations are higher and extend further for MM, but do not impact the mixed layer depth there, while for LL the deepest convection occurs at the sea ice edge in this region. HadGEM3-GC31-LL shows a significant warm bias across the hydrographic section, with very warm surface waters from the NAC and high temperatures extending throughout the Irminger and Iceland basins. The LL MLD corresponds best to CMEMS, even with slight temperature and salinity biases (the least out of all the models here).

In terms of future predictions, the LL model (panel a) shows a relatively weak decline throughout the 21st century (ending in 2050). For the MM model (panel b), the decrease is more significant (beginning the historical period at ~ 17 Sv and ending at ~ 12 Sv. This model overestimates the deep convection in the Labrador Sea and can potentially lead to a more severe impact on the AMOC if it were to suddenly decrease or stop completely. For the HH model (panel c), the AMOC strength decrease also significantly throughout the historical and future periods, from ~ 20 Sv in 1850 to 15 Sv in 2050 but was not studied in this work to test its validity.

5 Conclusion

The research question posed at the beginning of this thesis was: *How does the representation of circulation and hydrography influence deep convection in a range of CMIP6 models?* To answer this, temperature and salinity variables were shown throughout the SPNA, and the density stratification was calculated and compared to regions of deep convection. Biases in these variables can be caused by a stronger AMOC and sea ice concentration differences. Models with a stronger AMOC generally have higher SPNA temperatures and salinities, with lower sea ice concentrations, especially in the Labrador Sea, allowing for more deep convection in this region. Models with a weaker AMOC show higher sea ice concentrations in the Labrador Sea, with lower salinity and increased buoyancy, and no deep convection occurring in this region. Buoyancy loss from the summer to the winter largely determines the region of deep convection in the SPNA, which can occur through heat loss to the atmosphere by winds or the addition of colder or fresher waters. In the Nordic Seas, deep convection occurs at the sea ice edge (concentration > 50 %) for most models and CMEMS, with deep convection in the Labrador Sea not being accurately represented in all the models studied here. This reduces the reliability of future projections.

The issues in the climate models are not entirely due to resolution. The medium resolution HadGEM3-GC31-MM model convects in the correct region of the Labrador Sea but with too-deep mixed layer depths. In comparison, the lower resolution model HadGEM3-GC31-LL compares better to CMEMS in terms of mean mixed layer depth and location. While the reduction of AMOC strength throughout the 21st century is seen in all models, the model that most accurately represents deep convection in the SPNA is likely to be the most realistic. Out of the models studied here, this would be HadGEM3-GC31-LL, showing a decrease in AMOC strength throughout the 21st century, but a recovery for the lowest SSP scenario.

In the future, sea ice representation in climate models should be carefully considered, so as not bias the temperatures and salinities in the SPNA and causing stratification differences with reduced potential for deep convection. The link between the sea ice extent and the AMOC strength should be more closely analyzed to determine the influence of one over the other in models. While biases were not reduced in the higher resolution model, the convection in HadGEM3-GC31-MM shows promising results for the location of mixed layer depths and can hopefully be developed even further in future models to provide reliable climate projections.

Acknowledgements

I would, first of all, like to thank my supervisors Dr. Femke de Jong and Elodie Duyck from NIOZ for making the project available to me and for all the meetings and guidance throughout my thesis. I really appreciated your availability to talk and discuss new and interesting things every week, as well as all the help in the beginning getting to know the CMIP6 models and how to work with them in Python. Although I only came to NIOZ once a week, I am very grateful for the time spent there and the new people I have met in the OCS group. Secondly, I want to thank my UU supervisor, Dr. Peter Bijl for being enthusiastic about the project from the beginning and providing useful feedback.

I would also like to thank my mom and dad for the continuous love and support through all the highs and lows, I could not have come this far without you (grazie di tutto!). Finally, a huge thank you to my boyfriend, for always having the time for me and making me feel better when things aren't going my way.

Thank you to all of you for making this project possible, and I look forward to continuing to work in the field of physical oceanography and staying in contact in the future!

References

Aagaard, K., & Coachman, L. K. (1968a). The East Greenland Current north of Denmark Strait: Part I. *Arctic*, 181-200.

Aagaard, K., & Coachman, L. K. (1968b). the East Greenland current north of Denmark strait: Part II. *Arctic*, 267-290.

Bacon, S., Reverdin, G., Rigor, I. G., & Snaith, H. M. (2002). A freshwater jet on the east Greenland shelf. *Journal of Geophysical Research: Oceans*, *107*(C7), 5-1.

Bakker, P. (2022). Ocean sensitivity to freshwater. *Nature Climate Change*, *12*(5), 419-420.

Bethke, I.; Wang, Y.; Counillon, F.; Kimmritz, M.; Fransner, F.; Samuelsen, A.; Langehaug, … & Keenlyside, N. (2019). NCC NorCPM1 model output prepared for CMIP6 CMIP historical. Earth System Grid Federation.

Bethke, I., Wang, Y., Counillon, F., Keenlyside, N., Kimmritz, M., Fransner, F., ... & Eldevik, T. (2021). NorCPM1 and its contribution to CMIP6 DCPP. *Geoscientific Model Development*, *14*(11), 7073-7116.

Bi, D., Dix, M., Marsland, S., O'farrell, S., Sullivan, A., Bodman, R., ... & Heerdegen, A. (2020). Configuration and spin-up of ACCESS-CM2, the new generation Australian community climate and earth system simulator coupled model. *Journal of Southern Hemisphere Earth Systems Science*, *70*(1), 225-251.

Biló, T. C., Straneo, F., Holte, J., & Le Bras, I. A. (2022). Arrival of New great salinity anomaly weakens convection in the Irminger Sea. *Geophysical Research Letters*, *49*(11), e2022GL098857.

Buckley, M. W and Marshall, J. (2016). "Observations, inferences, and mechanisms of the Atlantic Meridional Overturning Circulation: A review". *Reviews of Geophysics* 54.1, pp. 5–63.

Danabasoglu, G., Lamarque, J. F., Bacmeister, J., Bailey, D. A., DuVivier, A. K., Edwards, J., ... & Strand, W. G. (2020). The community earth system model version 2 (CESM2). *Journal of Advances in Modeling Earth Systems*, *12*(2), e2019MS001916.

Danabasoglu, G. (2019). NCAR CESM2 model output prepared for CMIP6 CMIP historical. Earth System Grid Federation.

de Jong, M. F., Hendrik M van Aken, et al. (2012). "Convective mixing in the central Irminger Sea: 2002–2010". In: Deep Sea Research Part I: Oceanographic Research Papers 63, pp. 36–51.

de Jong, M. F., & de Steur, L. (2016). Strong winter cooling over the Irminger Sea in winter 2014–2015, exceptional deep convection, and the emergence of anomalously low SST. *Geophysical Research Letters*, *43*(13), 7106-7113.

de Jong, M. F., Oltmanns, M., Karstensen, J., & de Steur, L. (2018). Deep convection in the Irminger Sea observed with a dense mooring array. *Oceanography*, *31*(1), 50-59.

de Jong, M. F., de Steur, L., Fried, N., Bol, R., & Kritsotalakis, S. (2020). Year-round measurements of the Irminger Current: Variability of a two-core current system observed in 2014–2016. *Journal of Geophysical Research: Oceans*, *125*(10), e2020JC016193.

Dix, M.; Bi, D.; Dobrohotoff, P.; Fiedler, R.; Harman, I.; Law, R. … & Yang, R. (2019). CSIRO-ARCCSS ACCESS-CM2 model output prepared for CMIP6 CMIP historical. Earth System Grid Federation.

Duyck, E., Gelderloos, R., & de Jong, M. F. (2022). Wind-Driven Freshwater Export at Cape Farewell. *Journal of Geophysical Research: Oceans*, *127*(5), e2021JC018309.

Eyring, V., Bony, S., Meehl, G. A., Senior, C. A., Stevens, B., Stouffer, R. J., & Taylor, K. E. (2016). Overview of the Coupled Model Intercomparison Project Phase 6 (CMIP6) experimental design and organization. *Geoscientific Model Development*, *9*(5), 1937-1958.

Frajka-Williams, E., Bamber, J. L., & Våge, K. (2016). Greenland melt and the Atlantic meridional overturning circulation. *Oceanography*, *29*(4), 22-33.

Gelderloos, R., Straneo, F., & Katsman, C. A. (2012). Mechanisms behind the temporary shutdown of deep convection in the Labrador Sea: Lessons from the Great Salinity Anomaly years 1968–71. *Journal of Climate*, *25*(19), 6743-6755.

Gruber, N., Keeling, C. D., & Bates, N. R. (2002). Interannual variability in the North Atlantic Ocean carbon sink. *Science*, *298*(5602), 2374-2378.

González-Pola, C., Larsen, K. M. H., Fratantoni, P., and Beszczynska-Möller, A. (Eds.). 2020. ICES Report on Ocean Climate 2019. ICES Cooperative Research Reports No. 350. 136 pp.

Heuzé, C. (2021). Antarctic bottom water and North Atlantic deep water in cmip6 models. *Ocean Science*, *17*(1), 59-90.

Holte, J., Talley, L. D., Gilson, J., & Roemmich, D. (2017). An Argo mixed layer climatology and database. *Geophysical Research Letters*, *44*(11), 5618-5626.

IPCC, 2022: Climate Change 2022: Impacts, Adaptation and Vulnerability. Contribution of Working Group II to the Sixth Assessment Report of the Intergovernmental Panel on

Climate Change [H.-O. Pörtner, D.C. Roberts, M. Tignor, E.S. Poloczanska, K. Mintenbeck, A. Alegría, M. Craig, S. Langsdorf, S. Löschke, V. Möller, A. Okem, B. Rama (eds.)]. Cambridge University Press. Cambridge University Press, Cambridge, UK and New York, NY, USA, 3056 pp.

Jackson, L. C., Kahana, R., Graham, T., Ringer, M. A., Woollings, T., Mecking, J. V., & Wood, R. A. (2015). Global and European climate impacts of a slowdown of the AMOC in a high resolution GCM. *Climate dynamics*, *45*, 3299-3316.

Jackson, L. C., Roberts, M. J., Hewitt, H. T., Iovino, D., Koenigk, T., Meccia, V. L., ... & Wood, R. A. (2020). Impact of ocean resolution and mean state on the rate of AMOC weakening. *Climate Dynamics*, *55*(7), 1711-1732.

Jackson, L. C., & Petit, T. (2022). North Atlantic overturning and water mass transformation in CMIP6 models. *Climate Dynamics*, 1-21.

Killworth, P. D. (1983). Deep convection in the world ocean. *Reviews of Geophysics*, *21*(1), 1-26.

Kuhlbrodt, T., Griesel, A., Montoya, M., Levermann, A., Hofmann, M., & Rahmstorf, S. (2007). On the driving processes of the Atlantic meridional overturning circulation. *Reviews of Geophysics*, *45*(2).

Kuhlbrodt, T., Jones, C. G., Sellar, A., Storkey, D., Blockley, E., Stringer, M., ... & Walton, J. (2018). The low-resolution version of HadGEM3 GC3. 1: Development and evaluation for global climate. *Journal of Advances in Modeling Earth Systems*, *10*(11), 2865-2888.

Li, G., Cheng, L., Zhu, J., Trenberth, K. E., Mann, M. E., & Abraham, J. P. (2020). Increasing ocean stratification over the past half-century. *Nature Climate Change*, *10*(12), 1116-1123.

Lazier, J., Pickart, R., & Rhines, P. (2001). Deep convection. *International Geophysics*, *77*, 387-400.

Levermann, A., Bamber, J. L., Drijfhout, S., Ganopolski, A., Haeberli, W., Harris, N. R., ... & Weber, S. (2012). Potential climatic transitions with profound impact on Europe: Review of the current state of six 'tipping elements of the climate system'. *Climatic Change*, *110*, 845-878.

Lozier, M. S. (2012). Overturning in the north atlantic. *Annu. Rev. Mar. Sci*, *4*(1), 291-315.

Lozier, M S. et al. (2017). "Overturning in the Subpolar North Atlantic Program: A new international ocean observing system". In: Bulletin of the American Meteorological Society 98.4, pp. 737–752.

Lozier, M. S., Li, F., Bacon, S., Bahr, F., Bower, A. S., Cunningham, S. A., ... & Zhao, J. (2019). A sea change in our view of overturning in the subpolar North Atlantic. *Science*, *363*(6426), 516-521.

Marshall, J., & Schott, F. (1999). Open-ocean convection: Observations, theory, and models. *Reviews of geophysics*, *37*(1), 1-64.

McCarthy, G. D., Smeed, D. A., Cunningham, S. A., & Roberts, C. D. (2017). Atlantic meridional overturning circulation. *MCCIP Science Review 2017.*

McDougall, T. J., & Barker, P. M. (2011). Getting started with TEOS-10 and the Gibbs Seawater (GSW) oceanographic toolbox. *Scor/Iapso WG*, *127*(532), 1-28.

Pickart, R. S., Straneo, F., & Moore, G. K. (2003a). Is Labrador Sea water formed in the Irminger basin?. *Deep Sea Research Part I: Oceanographic Research Papers*, *50*(1), 23-52.

Pickart, R. S., Spall, M. A., Ribergaard, M. H., Moore, G. K., & Milliff, R. F. (2003b). Deep convection in the Irminger Sea forced by the Greenland tip jet. *Nature*, *424*(6945), 152-156.

Ridley, J.; Menary, M.; Kuhlbrodt, T.; Andrews, M.; Andrews, T. (2019a). MOHC HadGEM3-GC31-LL model output prepared for CMIP6 CMIP historical. Earth System Grid Federation.

Ridley, J.; Menary, M.; Kuhlbrodt, T.; Andrews, M.; Andrews, T. (2019). MOHC HadGEM3-GC31-MM model output prepared for CMIP6 CMIP historical. Earth System Grid Federation.

Sabine, C. L., Feely, R. A., Gruber, N., Key, R. M., Lee, K., Bullister, J. L., ... & Rios, A. F. (2004). The oceanic sink for anthropogenic CO2. *Science*, *305*(5682), 367-371.

Sgubin, G., Swingedouw, D., Drijfhout, S., Mary, Y., & Bennabi, A. (2017). Abrupt cooling over the North Atlantic in modern climate models. *Nature Communications*, *8*(1), 1-12.

Smeed D., Moat B.I., Rayner D., Johns W.E., Baringer M.O., Volkov D.L,. Frajka-Williams E.(2019). Atlantic meridional overturning circulation observed by the RAPID-MOCHA-WBTS (RAPID-Meridional Overturning Circulation and Heatflux Array-Western Boundary Time Series) array at 26N from 2004 to 2018. British Oceanographic Data Centre, National Oceanography Centre, NERC, UK.

Swart, N. C., Cole, J. N., Kharin, V. V., Lazare, M., Scinocca, J. F., Gillett, N. P., ... & Winter, B. (2019a). The Canadian earth system model version 5 (CanESM5. 0.3). *Geoscientific Model Development*, *12*(11), 4823-4873.

Swart, N. C., Cole, J. N.S., Kharin, V. V., Lazare, M.; Scinocca, J. F.; Gillett, N. P.; … & Sigmond, M. (2019b). CCCma CanESM5 model output prepared for CMIP6 CMIP historical. Earth System Grid Federation.

Talley, L. D. (2011). *Descriptive physical oceanography: an introduction*. Chapter S7. Academic press.

Thorpe, R. B., Gregory, J. M., Johns, T. C., Wood, R. A., & Mitchell, J. F. B. (2001). Mechanisms determining the Atlantic thermohaline circulation response to greenhouse gas forcing in a non-flux-adjusted coupled climate model. *Journal of Climate*, *14*(14), 3102-3116.

Trenberth, K. E., & Caron, J. M. (2001). Estimates of meridional atmosphere and ocean heat transports. *Journal of Climate*, *14*(16), 3433-3443.

Våge, K., Pickart, R. S., Moore, G. W. K., & Ribergaard, M. H. (2008). Winter mixed layer development in the central Irminger Sea: The effect of strong, intermittent wind events. *Journal of Physical Oceanography*, *38*(3), 541-565.

Våge, K., Pickart, et al. (2009). Surprising return of deep convection to the subpolar North Atlantic Ocean in winter 2007–2008. *Nature Geoscience*, *2*(1), 67-72.

Våge, K., Pickart, R. S., Sarafanov, A., Knutsen, Ø., Mercier, H., Lherminier, P., ... & Bacon, S. (2011). The Irminger Gyre: Circulation, convection, and interannual variability. *Deep Sea Research Part I: Oceanographic Research Papers*, *58*(5), 590-614.

Vreugdenhil, C. A., & Gayen, B. (2021). Ocean convection. *Fluids*, *6*(10), 360.

Weijer, W., Maltrud, M. E., Hecht, M. W., Dijkstra, H. A., & Kliphuis, M. A. (2012). Response of the Atlantic Ocean circulation to Greenland Ice Sheet melting in a strongly-eddying ocean model. *Geophysical Research Letters*, *39*(9).

Weijer, W., Cheng, W., Garuba, O. A., Hu, A., & Nadiga, B. T. (2020). CMIP6 models predict significant 21st century decline of the Atlantic meridional overturning circulation. *Geophysical Research Letters*, *47*(12), e2019GL086075.

Yang, Q., Dixon, T. H., Myers, P. G., Bonin, J., Chambers, D., Van Den Broeke, M. R., ... & Mortensen, J. (2016). Recent increases in Arctic freshwater flux affects Labrador Sea convection and Atlantic overturning circulation. *Nature communications*, *7*(1), 1-8.

Appendices

Appendix 1.1 Observational Data

Throughout this study, comparison of a range of CMIP6 models is performed with CMEMS reanalysis. Even though this has been validated (de Jong et al., 2020), deep convection in the Labrador Sea can be biased with respect to observations. Observational results are important to consider regarding the validity of certain models and their projections. The following figures show the observational data sets which can be used to compare spatial patterns of the models.

The OSNAP Array spans the Labrador (OSNAP West), Irminger and Iceland Basins and the Rockall Trough, with moorings located at various locations and depths Figure 21.

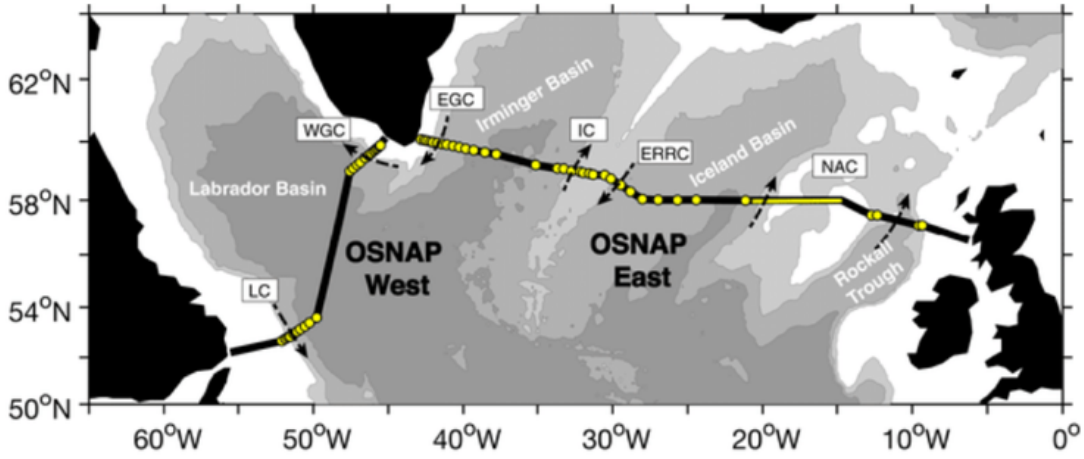

Figure 21: OSNAP East and West arrays. Locations of OSNAP mooring (yellow dots). Adapted from Li et al., 2021.

The OSNAP East array (from Cape Farewell at the southeast tip of Greenland to Scotland) has an overturning of 16.8 ± 0.6 Sv, while OSNAP West (spanning the Labrador Sea from the southern Labrador to southwest tip of Greenland) has 2.6 ± 0.3 Sv (for 2014-2016, e.g., Li et al., 2021; Lozier et al., 2019). See Li et al., 2021 for the mean meridional velocities and transports across the section.

Argo floats are also utilized throughout the world oceans and are useful for displaying the mixed layer depths throughout the SPNA. First, a figure from the ICES report on ocean climate (2019) is shown:

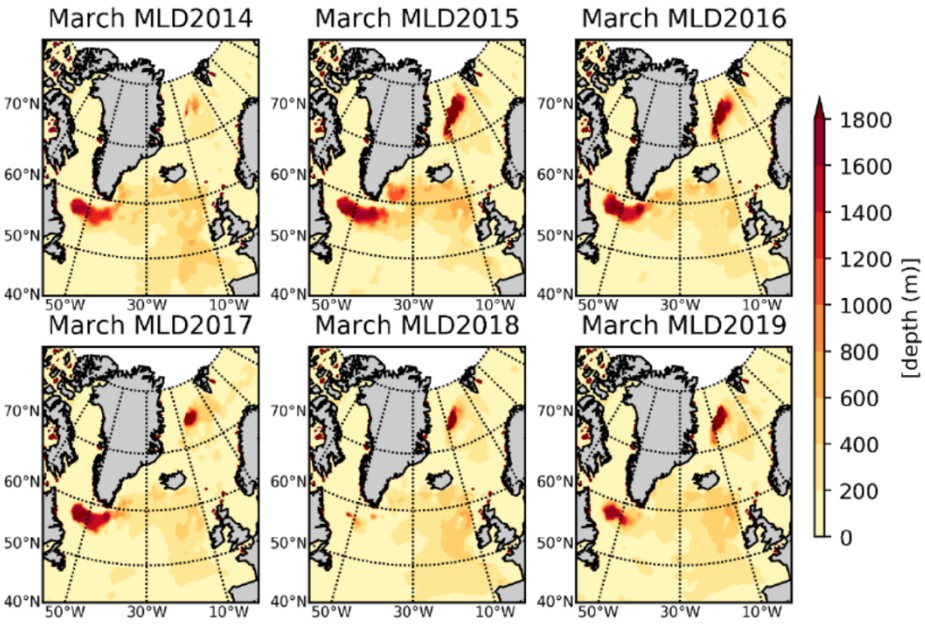

Figure 24: Maps of North Atlantic winter (March) mixed layer depths (MLD) for 2014 – 2019. From the ISAS monthly analysis of ARGO data. The mixed layer depth is defined as the depth at which the density has increased by more than 0.03 kg/m3 from the density at 10 m depth. This criterion is able to represent MLD in areas where there are both effects of temperature and salinity (ice melting). Source: González-Pola et al. (2020).

The mixed layer depth in the Labrador Sea can be more clearly shown in Figure 25, by Holte et al. (2017):

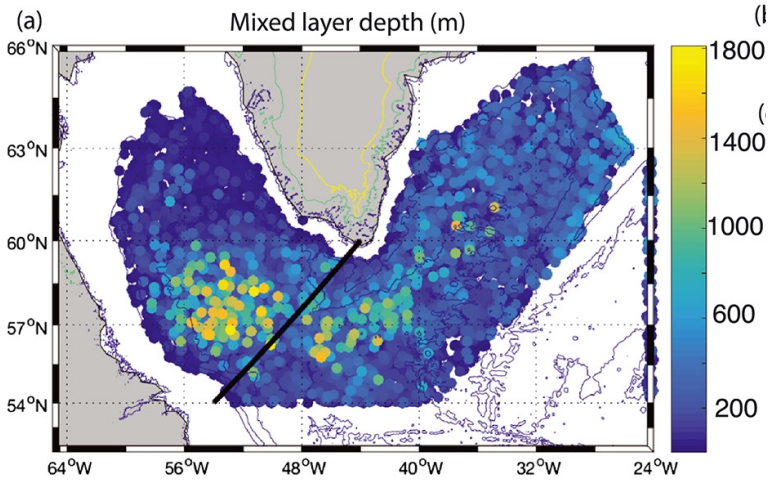

Figure 25: Map of algorithm MLDs from individual Argo profiles (colored dots). Adapted from Holte et al. (2017).

Appendix 1.2 Summer Variables

The summer sea surface temperature for the CMEMS reanalysis and models is shown below in Figure 23. This is used to compute the buoyancy (stratification) for the summer plots.

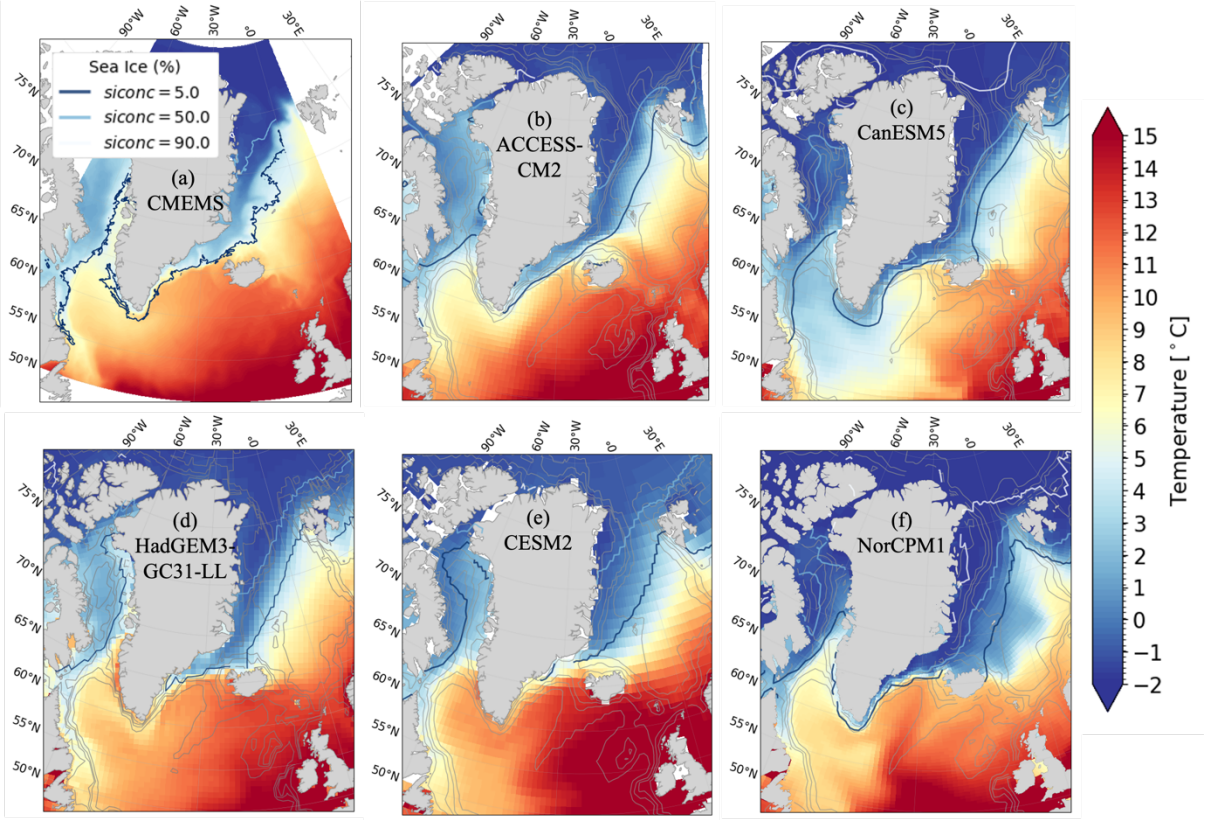

Figure 25: Mean summer (JAS) sea surface temperature (°C) for (a) CMEMS and (b-f) models.

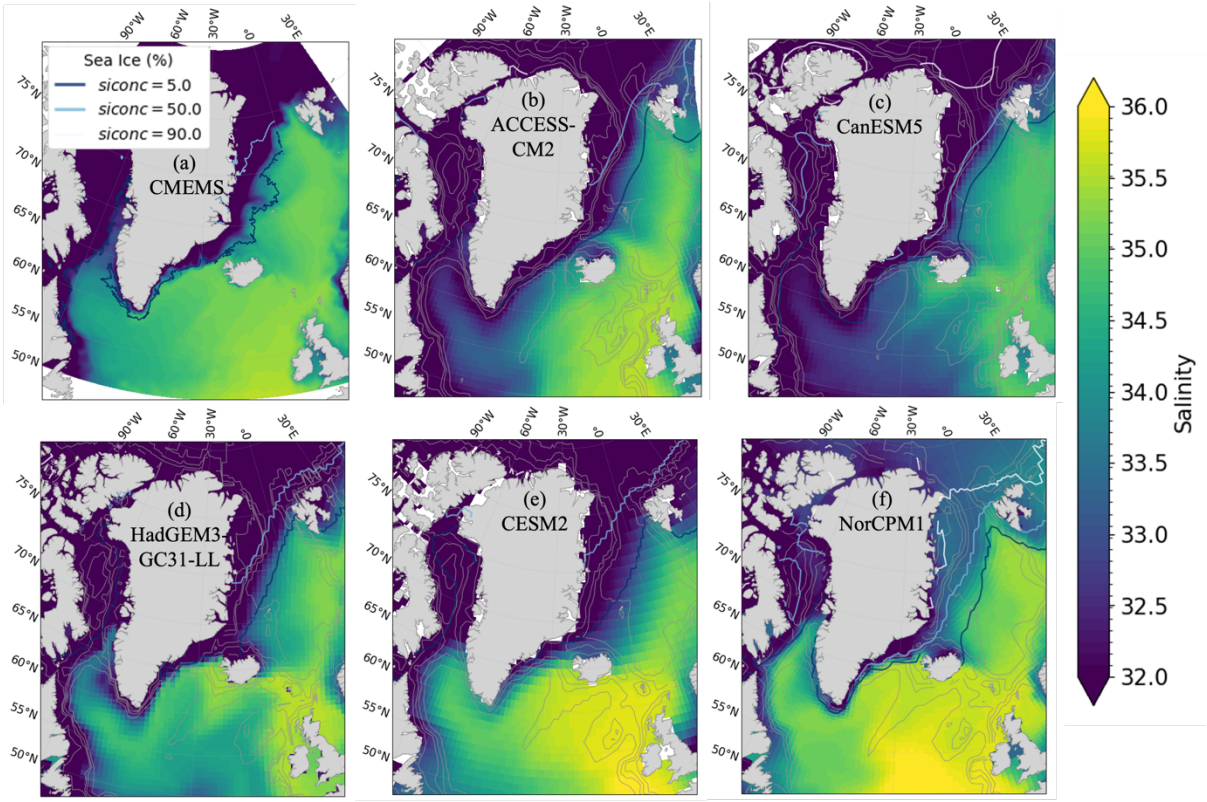

Figure 26: Mean summer (JAS) sea surface practical salinity for (a) CMEMS and (b-f) models.

Figure 27 shows the summer (JAS) buoyancy for the upper 500 m of the water column. HadGEM3-GC31-LL (left) and HadGEM3-GC31-MM.

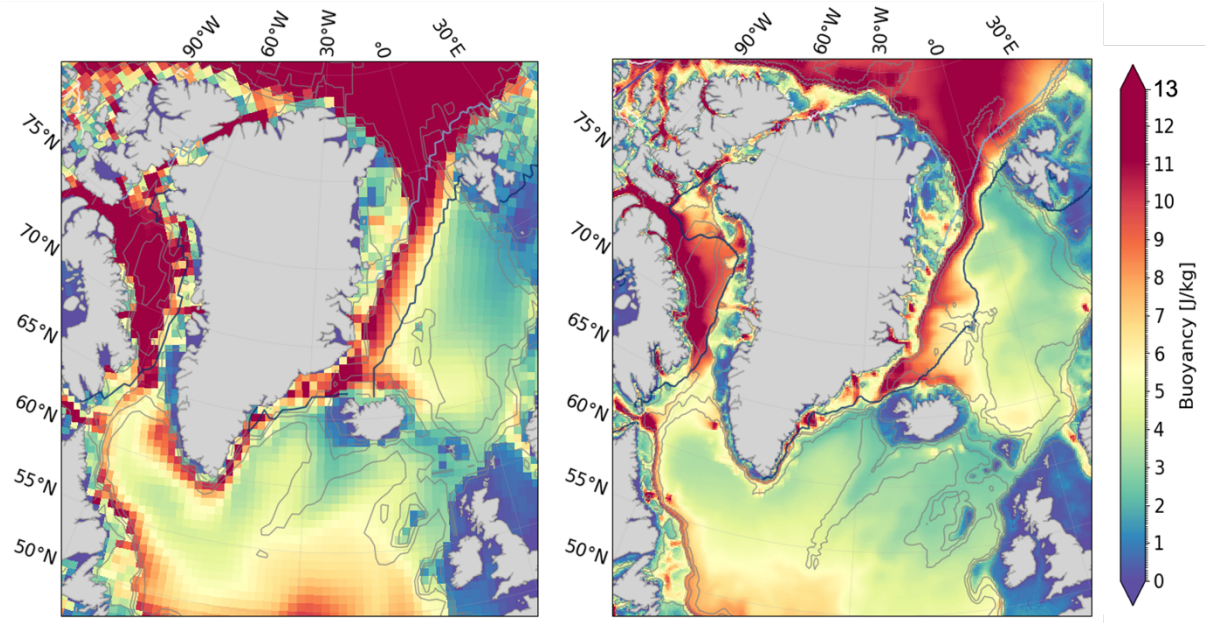

Figure 27: Summer (JAS) HadGEM3-GC31-LL (left) and HadGEM3-GC31-MM (right) buoyancy for the upper 500 m. Sea ice contours of 5 and 50 % shown in contour lines.